Polymerisation of Propene with Heterogeneous Ziegler-Natta Catalyst – Active Sites and Corresponding Polypropylene Structures

VILLE VIRKKUNEN

Laboratory of Polymer Chemistry
Department of Chemistry
University of Helsinki
Finland

ACADEMIC DISSERTATION

To be presented with the permission of the Faculty of Science of the University of Helsinki for public criticism in Auditorium A129 of the Department of Chemistry on 10th June 2005 at 12 o'clock

Helsinki 2005

Supervisor

Professor Franciska Sundholm
Laboratory of Polymer Chemistry
Department of Chemistry
University of Helsinki
Finland

Reviewers

Dr. Barbro Löfgren
Laboratory of Polymer Technology
Helsinki University of Technology
Finland

Professor Carl-Erik Wilén
Laboratory of Polymer Technology
Åbo Akademi
Finland

Opponent

Professor Ulf Gedde
Fibre and Polymer Technology
Royal Institute of Technology
Sweden

Custos

Professor Heikki Tenhu
Laboratory of Polymer Chemistry
Department of Chemistry
University of Helsinki
Finland

ISBN 952-91-8746-7 (paperback)
ISBN 952-10-2483-6 (pdf)
http://ethesis.helsinki.fi
Yliopistopaino
Helsinki 2005

Preface

This work was carried out in the Laboratory of Polymer Chemistry at the University of Helsinki between 2000 and 2005 in close collaboration with Borealis Polymers Oy. Financial support from the Magnus Ehrnrooth Foundation and the Finnish Cultural Foundation is gratefully acknowledged. CSC provided the computational resources.

I am most grateful to Professor Emerita Franciska Sundholm for the opportunity to work in this project and for her insight, guidance and encouragement. I also wish to thank the current Head of the Laboratory, Professor Heikki Tenhu, for making the laboratory such an agreeable workplace. I am indebted to Professor Sirkka Liisa Maunu for the help and expertise she offered when I was doing the NMR experiments.

Special thanks belong to Docent Lars-Olof Pietilä and Dr. Jaana Ennari for their help and valuable advice on molecular modelling. I am also very grateful to Professor Françoise Lauprêtre, Professor Anatoly Darinskii and Professor Tapani Pakkanen for valuable discussions and collaboration.

The initiative for this work came from Borealis Polymers Oy. I wish to thank everyone involved in the project: Päivi Pitkänen, Thomas Garoff, Torvald Vestberg, Pirjo Jääskeläinen and Arja Lehtinen. The cooperation was truly a source of joy.

I am grateful to all former and current researchers and workers in the Laboratory of Polymer Chemistry for making the laboratory a great place to work in. Special thanks to Hanne Wikberg and Tiina Lilja who shared a room with me, to Mikael Paronen for keeping spirits buoyed on the third floor, and to Heljä Heikkilä, Juha Solasaari, Marjut Wallner and Seija Lemettinen for their kind help in diverse matters.

Finally, I would like to thank my brother Iikka and my parents for the continuous encouragement and support during this work. Last but not least, dear Sari, without you this work would never have reached completion.

Helsinki, May 2005

Ville Virkkunen

Abstract

Commercial isotactic polypropylene is mainly produced with heterogeneous Ziegler-Natta catalysts. The heterogeneous nature of the catalyst system makes it extremely complex and difficult to study directly. In this work, a heterogeneous Ziegler-Natta catalyst was studied with DFT calculations and test polymerisations and indirectly through the characterisation and analysis of the polypropylene structure.

The effect of the external electron donor was studied with a series of polymers prepared with different TEA/ED ratios. An active site that alters state upon the coordination of an electron donor was found to explain the changes in the average activity, molar mass and isotacticity (^{13}C NMR).

DFT calculations were used to investigate the regiospecificity of a model catalyst site. In a catalyst generally considered regiospecific, the regioirregular addition is of interest in view of the proposed formation of dormant sites in this reaction. With the associated hydrogen activation effect, this reaction can influence both polymerisation activity and polymer structure. The calculations showed strong agostic interactions between the Ti of the active site and one of the hydrogens of the growing chain. These interactions were found to have a two-fold influence on the insertion reactions. The α-agostic interaction stabilised the transition structure and lowered the activation energy, while the β-agostic interaction effectively rendered the site inactive for propene insertion. These results are in agreement with the formation of dormant sites, and also help to explain the differences observed in ethene and propene polymerisations. In contrast to the result for propene, the β-agostic active site was active for ethene insertion.

For the measurement of tacticity distribution, the successive self-nucleation and annealing (SSA) method was applied for the first time to polypropylene. For the evaluation of the SSA method, two polypropylene samples, one with high and one with moderate isotacticity, were fractionated using a series of solvents with increasing boiling points and a series of increasing temperatures. Fractions were characterised by ^{13}C NMR, DSC, TREF and SEC. The ^{13}C NMR results were used to determine the stereosequences in the fractions, and these data, together with Monte Carlo based computer simulations, were further used to study and evaluate stochastic models with two to four active sites. The model C1+Es+CE1 gave the best result in terms of least-squares fit and the predicted crystallisable sequence lengths.

Abbreviations

C1	Propagation model with parameters σ_1, σ_2, P_{12}, P_{21}
CE	Chain-end control
CE1	Chain-end control, first-order Markovian
CPU	Central processing unit
DFT	Density functional theory
DSC	Differential scanning calorimetry
ED	External electron donor
Es	Enantiomorphic site control
EsCE	Propagation model with parameters P_r, σ, P_{12}, P_{21}
ID	Internal electron donor
iPP	Isotactic polypropylene
MAO	Methylaluminoxane
MFR	Melt flow rate
MRL	Meso run length
NMR	Nuclear magnetic resonance
PP	Polypropylene
SAXS	Small-angle X-ray scattering
SEC	Size exclusion chromatography
SIST	Stepwise isothermal segregation technique
SSA	Successive self-nucleation and annealing
TEA	Triethylaluminium
TREF	Temperature rising elution fractionation
Z-N	Ziegler-Natta
XS	Xylene soluble fraction

Symbols

C_p	Heat capacity
β	Heating rate
Δh_f^0	Specific enthalpy of fusion
l_c	Lamellar thickness
$\overline{M_n}$	Number average molar mass
$\overline{M_w}$	Weight average molar mass
P_x	Probability for the formation of a x-diad, where x is *m* for meso diad and *r* for racemo diad. (CE model)
P_{xy}	Probability for the formation of a y-diad, following an x-diad, where y and x are *m* for meso diad and *r* for racemo diad (CE1 model)
P_{ij}	Probability for switching from state i to state j (C1 and EsCE models)
P_{tr}	Probability for chain termination in the Monte Carlo simulation
r	Chain length
ρ_c	Crystal density
σ_{fr}	Surface free-energy
σ	Probability for the selection of the R or S enantioface of a prochiral monomer (Es model)
T_c	Crystallisation temperature
T_m	Melting temperature
T_m^0	Equilibrium melting temperature
τ	Ratio of chain transfer rate to propagation rate

List of Original Publications

This thesis is based on the following original papers, hereafter referred to by the corresponding Roman numerals. Some new material is presented.

I. **A qualitative model for polymerisation of propylene with a $MgCl_2$-supported $TiCl_4$ Ziegler–Natta catalyst**, T. Garoff, V. Virkkunen, P. Jääskeläinen, T. Vestberg, *European Polymer Journal*, (2003), **39**, 1679.

II. **DFT investigation of the regiospecificity of a model catalyst site for propene polymerisation**, V. Virkkunen, L.-O. Pietilä, F. Sundholm, *Polymer*, (2003), **44**, 3133.

III. **Tacticity distribution of isotactic polypropylene prepared with heterogeneous Ziegler –Natta catalyst. 1. Fractionation of polypropylene**, V. Virkkunen, P. Laari, P. Pitkänen, F. Sundholm, *Polymer*, (2004), **45**, 3091.

IV. **Tacticity distribution of isotactic polypropylene prepared with heterogeneous Ziegler –Natta catalyst. 2. Application and analysis of SSA data for polypropylene**, V. Virkkunen, P. Laari, P. Pitkänen, F. Sundholm, *Polymer*, (2004), **45**, 4623.

Author's Contribution to the Publications

Publication I

Ville Virkkunen was responsible for the literature review. The original plan was that of Thomas Garoff. The experimental work was performed at the R&D laboratories of Borealis Polymers Oy, Porvoo. The discussion and conclusion sections were written in cooperation with the other authors.

Publication II

Ville Virkkunen drew up the original work plan, performed all the calculations and wrote the manuscript.

Publications III and IV

Ville Virkkunen provided the original idea for these studies and drew up the research plan. Pasi Laari carried out the fractionations. Ville Virkkunen wrote the manuscripts.

Table of Contents

1 Introduction

Polypropylene (PP) is one of the fastest growing commodity plastics in the world today. According to a conservative estimate, the global market is growing at an average rate of 3% a year and consumption is estimated to reach 33 Mt annually by 2005.[1] With the total amount of plastics produced each year in the neighbourhood of 150 Mt (in 1997), the importance of PP is clear. The growth is due to the excellent properties and wide applicability of polypropylene, which have enabled it to successfully challenge other materials on the market. The term polypropylene actually refers to a class of materials with divergent properties, the only common denominator being the monomer. The many grades of polypropylene are variously used in the manufacture of fibres, food packages, household appliances and consumer products, construction products such as pipes, and a host of components for the automotive industry, including dashboards and bumpers.

Most polypropylene today is manufactured with traditional heterogeneous Ziegler-Natta (Z-N) catalysts, the type with which Giulio Natta initially produced crystalline polypropylene in 1954. Polypropylene was the first synthetic highly stereoregular polymer.[2] As was predicted even before the structure was proven, it was the stereoregularity of the polymer that allowed it to crystallise.[3] As was the case in the first syntheses, the catalyst is still the key to the successful preparation of isotactic, stereoregular polypropylene.

Along with the heterogeneous catalyst, polypropylene is now also produced with homogeneous metallocene catalysts.[4] Although these catalysts were originally developed in the 1950s, it was not until the discovery of methylaluminoxane (MAO) as an activator[5] that the current intense research in the field began. With homogeneous catalysts, the two major shortcomings of traditional heterogeneous Ziegler-Natta catalysts – the presence of multiple active sites and the high sensitivity to heteroatoms – can be avoided. Because they contain only a single active site the homogeneous catalysts provide much finer control over the final product. Moreover, tailoring of the ligand framework of the catalyst has opened the way to the preparation of completely new polymers. At the same time, developments in late transition metal catalysts have shown that the limitation of Z-N catalysts to polymerise only vinyl monomers can, in fact, be overcome.[6, 7]

Despite these new and interesting developments in the field, it is predicted that traditional heterogeneous Z-N catalysts will dominate the markets for several years to come.[4] Among the reasons for this are the excellent processing properties of Z-N polypropylene with its wide molar mass distribution and lower production costs. The present study was driven by the need to better understand and control polymerisation processes that are based on the complex heterogeneous Z-N catalyst system.

1.1 Scope of the Work

This thesis summarises studies on propene polymerisation, polypropylene structure and modelling of the polymerisation mechanism with a heterogeneous Ziegler-Natta catalyst. The main interest was to obtain a better understanding of the reactions that govern the polymer structure and ultimately to model these effects. As mentioned above, the presence of multiple active sites in the catalyst is a major shortcoming of this otherwise successful heterogeneous catalyst system. In prediction of the polymer structure, knowledge of the different types of active sites and of their characteristics is essential. Despite countless investigations in the field, the exact structure, characteristics and number of the different active sites remain under debate. The difficulty in obtaining reliable direct information about the catalyst suggests that alternative methods of investigation are needed. In this work the Z-N catalyst system was studied by methods of computational chemistry and indirectly through characterisation and analysis of the polypropylene structure and tacticity distribution by calorimetric methods. For the measurement of tacticity distribution the successive self-nucleation and annealing method is for the first time applied to polypropylene. Computer simulations together with NMR and DSC data are used to study and evaluate complex active site models.

2 Heterogeneous Ziegler-Natta Catalysts

The development and structure of heterogeneous Ziegler-Natta catalysts have been described in many books and reviews.[8, 9, 10] In the following, I present a short description of the catalyst, followed by reviews of the polymerisation mechanism, the active site structure and recent computational studies.

A Ziegler-Natta catalyst is derived from a transition-metal halide and a metal hydride or metal alkyl. Modern Ziegler-Natta catalysts for propene polymerisation contain $TiCl_4$ supported on $MgCl_2$. The catalyst is activated with the metal alkyl, triethylaluminium (TEA) and, in addition, two electron donors, one internal and one external, are typically used. The internal electron donor (ID) is added during the preparation of the catalyst and the external donor (ED) is complexed with the cocatalyst (TEA) prior to activation. In fourth generation catalysts, the internal donor is a diester and the external donor an alkoxysilane.[11] In most $MgCl_2$-based catalysts the ID content follows the content of Ti. The ID/Ti molar ratio is normally between 0.77 and 0.82.[12] The amount of external donor, or more commonly the Al/ED ratio, is an adjustable parameter in the polymerisation, which is used to control the stereospecificity of the catalyst. Recent improvements in polypropylene catalysts can mainly be attributed to the development of new and more efficient electron donors.[13, 14, 15] Although the mechanism by which the electron donors modify the active sites is not completely understood, the influence on the stereospecificity of the catalyst is clear. Table 1 lists some electron donors and the respective isotacticities that can be achieved in propene polymerisation.[11]

Table 1 *Internal and external electron donors used in heterogeneous Z-N catalysts and the isotacticities obtained with these catalysts.*[11]

Electron donors (ID+ED)	Isotacticity (wt.-%)
-	< 50
ethylbenzoate + methyl-*p*-toluate	90-95
alkylphthalates + alkoxysilanes	95-99
1,3-diethers	95-99

2.1 Polymerisation Mechanism

Cossee and Arlman[16, 17, 18] have proposed the commonly accepted model for the reaction pathway of α-olefin insertion in Ziegler-Natta catalysts (originally for α-$TiCl_3$). In this model, an octahedrally coordinated transition metal ion with one vacant coordination position and one alkyl group in its coordination sphere forms the active site. The role of the cocatalyst is solely to alkylate the active site and act as a scavenger. The π-bond of the monomeric olefin coordinates to the vacant position, weakening the transition metal–carbon bond, and the olefin is inserted between the transition metal and carbon. The insertion proceeds through a four-member transition state involving the Ti-C bond and the carbons of the olefin double bond.

An important modification to this scheme was presented by Brookhart et al.[19] Introducing the term agostic to describe carbon–hydrogen bonds acting as ligands to transition metal centres, they suggested that the α-hydrogen of the growing alkyl chain could form a C–H – Ti bridge. This mechanism with the agostically stabilised transition state is shown in Scheme 1. The strong agostic stabilisation has been confirmed in theoretical calculations. [20, 21]

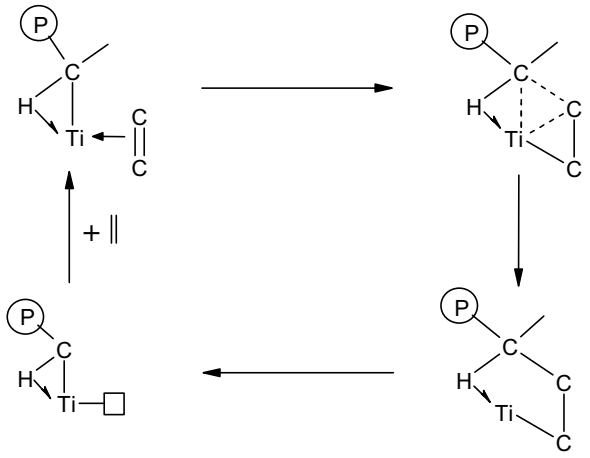

Scheme 1 *Reaction mechanism in olefin insertion according to Brookhart et al.*[19]

Stereoregular polymerisation in the Cossee–Arlman[18] scheme is explained with a shift of the growing chain back to the original position after each insertion. This guarantees that successive monomer insertions occur from the same side of the enantioselective active site. Allegra[22] and Corradini and co-workers[23, 24, 25] have presented models that, because of C_2 symmetry in the active site, do not require the chain back-jump to maintain selectivity. In the Corradini model, the stereoselectivity of the insertion depends crucially on the orientation of the growing chain.

2.2 Active Sites in $MgCl_2$-supported Catalysts

The activated $MgCl_2$ support consists of small crystallites with surfaces containing coordinatively unsaturated Mg ions. The most widely studied surfaces are (110) and (100), which are the representative surfaces for 4- and 5-coordinated Mg, respectively.[11, 26] When the catalyst is activated, the coordinated $TiCl_4$ on the different $MgCl_2$ crystal planes creates active sites with different Lewis acidic strengths, sterical hindrances and titanium oxidation states. The activation of the catalyst involves alkylation and reduction of titanium. The distribution of titanium oxidation states in activated Z-N catalysts varies, but considerable amounts of Ti(II), Ti(III) and Ti(IV)

states have been found.[27] Commonly it is considered that Ti(III) forms the active site in propene polymerisation.[25, 28] However, Ti(II) has also been shown to be active,[29] despite earlier reports suggesting that it is only active in ethene polymerisation.[30, 31]

In the Corradini[25] model, Ti_2Cl_6 dimers, which are coordinated to the edges of a $MgCl_2$ crystal on the (100) plane of $MgCl_2$, form the stereospecific active sites in the catalyst. These sites resemble the active sites described for the first generation $TiCl_3$-based Z-N catalysts. There is also evidence to suggest that a catalyst prepared from support material having prevalently (100) planes is more stereospecific than one prepared from a support that contains both (100) and (110) planes.[32]

Without electron donors, $MgCl_2$-supported Z-N catalysts are not very stereospecific in propene polymerisation.[11] In the above active site model, the role of the electron donors is to compete with $TiCl_4$ for the coordination on the (110) plane of $MgCl_2$,[25] since the coordination of $TiCl_4$ on this plane would create undesired non-stereospecific sites. Several other models suggest that the role of the electron donors in the polymerisation is more direct. In particular increases in the production of stereoregular polymer and variations in molar mass and molar mass distribution with the electron donor or electron donor type have been explained with models that involve the formation of new sites. [33, 34, 35, 36] In these models, selective deactivation of the non-stereospecific sites is due to the electron donors favouring coordination on the more Lewis acidic, non-stereospecific, sites.[37] According to Soga et al.,[38] coordination of an electron donor to a non-stereospecific site with two open coordination places will result in an isospecific site with only one vacancy.

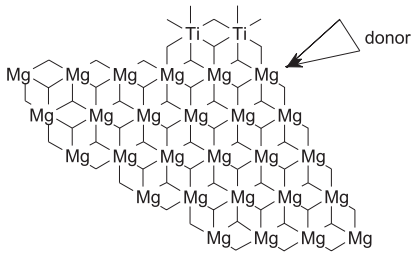

Figure 1 *The position of a donor on a 4-coordinated Mg in the $MgCl_2$ crystal according to Barino et al.*[39]

Barino et al.[39, 40] have presented models that explain the formation of new stereospecific sites without direct coordination of the donors to the active sites. They found a correlation between the efficiency of electron donors to promote stereoregular polymerisation and their preferential coordination on the (110) plane of $MgCl_2$ in accordance with the Corradini model. Recognising that good supports are always defective, they demonstrated several positions on the $MgCl_2$ surface where coordination

of a donor near a non-stereospecific active site can sterically create the required symmetry of a stereospecific site (Figure 1).

The most recent models propose active sites that fluctuate between stereospecific and less stereospecific states.[41, 42]

2.3 Computational Catalyst Studies

Ziegler-Natta catalysts have been investigated extensively by computational methods, though far less than homogeneous catalysts (see, for example, refs. 43 and 44 and references therein). The main reason for this is the complexity of the heterogeneous system. In principle, calculations require very large models and significant CPU resources. As a result, most calculations have been done with small model systems, and only very recently have all-electron calculations been reported. The investigations can be roughly divided into active site structure ($MgCl_2$ structure, $TiCl_4$ coordination) studies[20, 26, 39, 45, 46, 47, 48, 49, 50] and studies on the monomer coordination or polymerisation reaction. [20, 21, 47, 51, 52] Some studies have also been done on the cocatalyst[53, 54] and coordination of the electron donors. [40, 55, 56, 57, 58, 59]

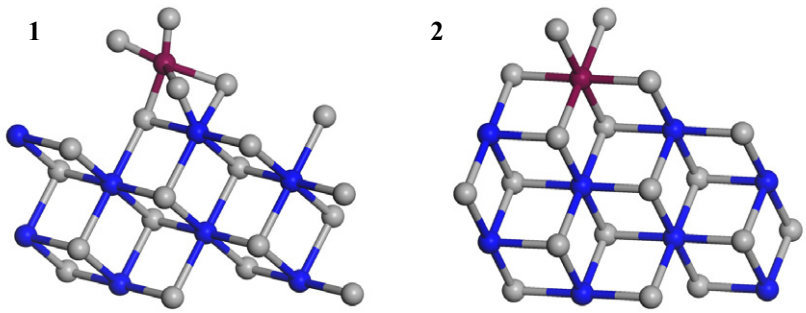

Figure 2 *Active sites on 4-coordinated $MgCl_2$ surface: 5-fold site (**1**) and the 6-fold Corradini site (**2**).*

2.3.1 $TiCl_4$ Coordination on $MgCl_2$ Support

$TiCl_4$ coordination on $MgCl_2$ support has been studied by Colbourn et al.,[45] Puhakka et al.,[46] Gale et al.[51] and most recently by Monaco et al.[50] and Boero and co-workers.[20, 26, 47, 48, 52] Gale et al.[51] found that the most likely binding site for $TiCl_4$ is on the (100) surface of $MgCl_2$. The more recent results,[26, 50] however, suggest that coordination of mononuclear $TiCl_4$ is only possible on the (110) surface, where $MgCl_2$ is four coordinated. Boero's group found two possible Ti adducts, one (Figure 2, **1**) corresponding to the 5-fold site first identified by Puhakka et al.[46] and the other to the Corradini (mononuclear) model (**2**). Monaco et al.[50] obtained similar results: coordination of mononuclear $TiCl_4$ and $TiCl_3$ is favoured on the (110) surface, whereas

on the (100) surface, coordination of dimeric Ti_2Cl_8 is favoured over mononuclear Ti species, but coordination of Ti_2Cl_6 is disfavoured. The authors were unable, however, to obtain a stable 5-fold site (similar to the one reported by Puhakka et al.[46] and Boero and co-workers[20, 26, 47]) with gradient-corrected functionals. Boero's group used local density approximation in the dynamics and only checked the optimised structures with gradient corrected functionals.

Boero et al.[26] have also reported calculations with binuclear Ti species. They studied Ti_2Cl_6 coordination on the 4-coordinated and 5-coordinated $MgCl_2$ surfaces. The coordination of Ti_2Cl_6 on the 5-coordinated $MgCl_2$ surface corresponds to the model Corradini et al.[25] presented, and this site was found to be stable but highly constrained. The binuclear adduct formed on the (110) surface was found to be significantly more stable. Interestingly, Boero et al.[26] found neither of these binuclear species to be stable in a polymerisation reaction, but reported that they break apart in a disproportionation reaction: 2Ti(III) → Ti(II) + Ti(IV). In the former case the Ti(IV) species is freed, while in the latter a site identical with the mononuclear 5-fold site on the (110) surface is formed. The Ti(II) species remains weakly attached to the support.

In accordance with the above result, Boero et al.[26] reported that a typical electron donor (di-*n*-butyl-phthalate) coordinates more strongly on the (100) surface than the (110) surface of $MgCl_2$. On the (110) surface, only a singly bound structure was obtained for the bidentate donor. They also showed that the Mg–Ti distance in the mononuclear Corradini site ((110) surface) corresponds closely to the Mg–Mg distance on the (100) surface. It is not surprising, therefore, that the donor molecule can coordinate to this non-stereospecific site and deactivate it. Using a combination of molecular mechanics and semiempirical methods, Toto et al.[58] obtained an opposite result for 1,3-diethers, which were found to bind more strongly on the (110) plane.

2.3.2 Polymerisation Reaction

The most recent computational studies on the polymerisation reaction in Ziegler-Natta catalysts are those of Cavallo et al.[21] and Boero et al. [26, 47, 48, 52] Cavallo's group studied polymerisation and termination reactions with ethene, while Boero's did extensive studies on ethene insertion to both the 5- and 6-fold sites and propene insertion to the 5-fold site in Figure 2. In the latter case, also 2,1 insertion was studied and found to be disfavoured. The 5-fold site (Figure 2, **1**) was active for both ethene and propene and also highly stereospecific in the latter case. In ethene polymerisation the 5-fold site was significantly more active than the Corradini site.

In both of the above studies the insertion reaction was found to be agostically assisted, in accordance with the suggestion of Brookhart et al.[19] However, Boero et al.[52] found that ethene insertion changes from α- to β-agostic after the first insertion (5-fold site). In the case of propene, also the second insertion was α-agostically assisted.

Both studies demonstrated that, contrary to the original Cossee-Arlman scheme, there is no back-jump of the chain. Cavallo et al.[21] found that the chain orients itself in an axis between the two octahedral positions when there is no coordinated monomer. In the case of a C_2-symmetric site, like the one suggested by Allegra et al.,[22] this does not influence the stereospecificity of the polymerisation. For the 5-fold site, Boero et al.[52] found that the chain grows roughly parallel to the substrate, always leaving the active site open from the same side. In this site the stereospecificity is due to the local geometry of the active site with the growing chain, in accordance with the model presented by Corradini et al.[23-25]

3 Polypropylene Structure

If we consider the polymer chain alone, polypropylene is one of the simplest polymers known: a carbon chain with a methyl group attached to every second carbon of the chain. The versatility of the polymer arises from the successive stereoconfigurations of the methyl groups. If the configurations are random, the material is amorphous, soft and sticky. If they are identical (isotactic structure), a semicrystalline material with excellent mechanical properties is obtained. Through tailoring of the chain structure, modifications of the crystalline structure and morphology and, in the end, of the material properties of the polymer can be achieved. The structure of the polymer also gives information about the catalyst system that produced it. As with all synthetic polymers, the structure of polypropylene can only be described with average values or distributions. In a typical case, the distributions can be derived from the statistical nature of the polymerisation reaction. In the case of Z-N polypropylene, the interpretation of the polymerisation results is more challenging because the polypropylene product is always a mixture of the polymers produced by the different active sites in the catalyst.

3.1 Molar Mass

Both molar mass and its distribution have a significant effect on the properties of polypropylene. The weight average molar masses of commercial polypropylenes typically range between 300 000 and 700 000.[60] The molar mass distributions of Z-N polypropylenes are broad with polydispersities ranging from 4 to 10.[60] In contrast, the width of the molar mass distribution of polymer produced with a single active site is ideally 2, as given by the Flory most probable distribution (Equation 1, Figure 3). [61]

$$w(r) = r\tau^2 e^{-r\tau} \tag{1}$$

In equation 1, r is the polymer chain length and τ is the ratio of the chain transfer rate to the propagation rate. It is evident from Figure 3 that active sites with significantly different ratios of the propagation rate to the chain transfer rate are present in the catalyst.

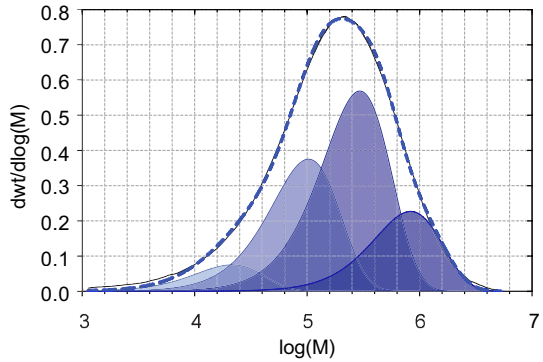

Figure 3 *Molar mass distribution of a PP sample measured with size exclusion chromatography and its deconvolution to four Flory most probable distributions that present the contribution of a single active site.*

3.2 Stereoregularity and Crystal Structure

Stereoregularity is a requirement for the crystallisation of polypropylene.[3] This makes isotacticity one of the key properties of polypropylene and the parameter that most heavily determines the crystallisation temperature, melting temperature and crystallinity.[62] Modern Ziegler-Natta catalysts can produce polymer with isotacticity reaching 99.0%. Although the degree of isotacticity can be determined by various methods, only ^{13}C NMR measurement gives direct information on the stereoconfigurations of the methyl groups along the chain. More precisely, from the ^{13}C NMR spectra of polypropylene it is possible to resolve the abundances of short sequences of meso and racemo placements of the monomers. The percentage of meso pentad (*mmmm-%*) is usually taken as a measure of average isotacticity. Especially in the case of Z-N PP, however, the average isotacticity does not always sufficiently characterise the polymer. Analysis of the distribution of isotacticity requires fractionation of the polymer. ^{13}C NMR sequence data can also be used for best-fit calculations of stochastic active site models.

In the following I review the stochastic models, crystalline morphology of polypropylene, polymer crystallisation models and methods for fractionation.

3.2.1 Stochastic Models

Stochastic models are commonly used in the interpretation of ^{13}C NMR sequence data. The two simplest models are the Markovian models of chain propagation: *chain-end-controlled propagation* (CE) and *site-controlled propagation* or *enantiomorphic site* (Es). In the CE model, the last inserted monomer determines the selectivity in the insertion of a new monomer unit. The Es model, in turn, assumes that the catalyst contains a racemic mixture of catalyst sites with opposite chiralities, which favour

monomers with opposite enantiofaces. In the CE model, the parameters P_r and $P_m = 1\text{-}P_r$ determine the probabilities for the formation of racemo and meso diads, respectively. In the Es model, σ and $(1\text{-}\sigma)$ give the probabilities for the selection of the opposite enantiofaces of a prochiral monomer. For the CE model, $P_r = 0.5$ results in atactic, $P_r > 0.5$ in syndiotactic and $P_r < 0.5$ in isotactic polymer. For the Es model, $\sigma = 0.5$ results in atactic polymer, and isotactic polymer is obtained when $\sigma \rightarrow 0.0$ or $\sigma \rightarrow 1.0$.

As mentioned above, sites that can be described with combinations of these two control mechanisms have also been proposed. Propagation models for these fluctuating sites, which produce stereoblock copolymer, have been introduced by Coleman and Fox[63] and later by Cheng et al.[64] As recently reviewed by Busico et al.,[65, 66] stochastic models can conveniently be described with transition matrices. The advantage of this formalism is that even complex multi-site models can easily be constructed and the resulting stereosequence probabilities can be solved numerically.

The distribution of stereosequences in Z-N PP cannot be described with any of the above stochastic models alone. To obtain a better fit with the experimentally measured stereosequence distributions, several authors have proposed two- and three-site models,[41, 42, 67, 68, 69, 70, 71] in which the above models are combined to account for the symmetric and asymmetric chains found in polypropylene. With the number of sites, also the number of adjustable parameters in the models increases. Already with three sites the number of parameters is at least five, which means that high-resolution ^{13}C NMR data is required for a reliable fit.[42] With hexad/nonad sequence data, Busico et al.[42] found a best-fit with a model containing the components Es, CE and C1, where C1 is a site that can switch between two states that follow Es statistics. The C1 component is needed to correctly predict the amount of m_xrmrm_y sequences that arise from consecutive stereoerrors. The amount of m_xrmrm_y sequences is overestimated with an Es+CE model. The Es+C1+CE model contains seven adjustable parameters after the constraint $\sigma(Es) = \sigma_1(C1)$ is added. The same three-site model describes both "atactic" and "isotactic" fractions of PP, which indicates that Z-N PP can be classified as a stereoblock copolymer with both defective and stereoregular sequences present in pentane soluble and insoluble fractions. The same conclusion was drawn by Alamo et al.[67, 72] on the basis of the similarity of the linear growth rates measured for Z-N PP fractions with different defect concentrations. The authors pointed out that complex three-site models cannot be distinguished solely by comparing the experimental and calculated stereosequence distributions but that the result must also be in agreement with the crystallisation data. Randall et al.[70] showed that the Es+C1+CE1 model is in better agreement with growth rate measurements than the three-site model proposed by Busico et al.[42] The only difference between these models is that Randall et al. used first-order Markovian statistics in the chain-end control component (CE1).

3.2.2 Polypropylene Crystal Morphology

Polypropylene crystallises in four different polymorphs (smectic, γ, β and α). Among these, the monoclinic α-form is predominant.[73, 74] The crystallographic unit cell, which defines the polymorph, is the smallest unit in the morphology of the polymer material. The next unit is the lamella which is formed when the helical chains pack and fold. As shown in Figure 4, the lamellae form stacks containing alternating layers of crystalline and amorphous phases. The formation of lamellae occurs in crystallisation from both melt and solution. However, it is thought that the folding in the lamellae is more irregular when crystallisation has occurred from melt rather than solution.[75] The final unit in the hierarchy is a spherulite which is a spherical aggregate of the lamellae. A special feature of polypropylene is the formation of cross-hatched texture in the spherulites of the α-monoclinic polymorph. In these spherulites, in addition to radial (R) lamellae, also tangential (T) lamellae are present, which cross the R lamellae at an angle of 100°. Yamada et al.[76] have shown that the degree of cross-hatching decreases with increasing isotacticity and T_c.

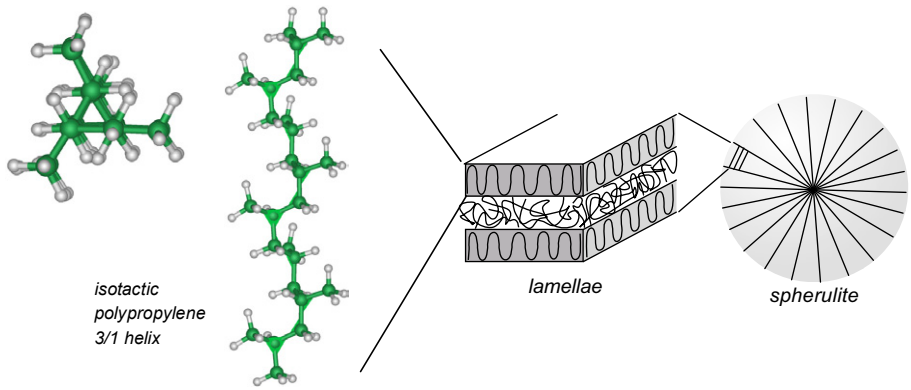

Figure 4 *Constituents of crystalline morphology of polypropylene.*

3.2.3 Crystallisation Models

Our understanding of the process of crystallisation in polymers continues to evolve. Typically, the crystallisation is described as a stepwise process of addition of chain stems into a growing crystal face. The crystallisation rates in this scheme are explained with three regimes of crystal growth. The models are described as kinetic (Hoffman-Lauritzen[77, 78]) or entropic (Sadler-Keller[79, 80]) depending on the origin of the energy barrier for the addition of a chain stem to the growth face. Recently, a growing amount of evidence has accumulated to suggest that the crystallisation in polymers involves several distinct phases or steps, i.e. at least in the bulk some kind of preordering occurs before crystallisation. Strobl et al.[81] have suggested that the crystallisation process in polymers involves the successive formation of isotropic melt, mesomorphic layer,

granular crystal layer and finally the lamellar crystal. In the case of polypropylene and other chiral but racemic polymers, this scheme has been disputed,[82] however, because it is unable to satisfactorily explain the crystallisation with the constraints that the selection of chiral chains imposes.[82] In the α and γ forms of polypropylene the alternating ordering of the left-handed and right-handed helices indicates that the crystallisation in polypropylene must be a substrate determined, sequential and local process.[82] The stringent requirement for the alternating chiralities of the chains and the molecular sorting out that this structure implies suggests that this growth mechanism which is based on condensation or deposition of pseudo-crystalline precursors, does not apply to polypropylene.[82]

A key step in the crystallisation of a polymer is the folding of the chains to form lamellae. In general, the fold length, or lamellar thickness (l_c), increases with the crystallisation temperature (T_c). According to the Thomson–Gibbs equation (2), the melting temperature (T_m) and l_c are related as

$$T_m = T_m^0\left(1 - \frac{2\sigma_{fr}}{l_c \rho_c \Delta h_f^0}\right) \tag{2}$$

In equation (2), T_m^0 is the equilibrium melting temperature, Δh_f^0 is the specific enthalpy of fusion, ρ_c is the crystal density and σ_{fr} is the surface free-energy. According to Flory,[83] the lamellar thickness in copolymers also depends on the amount of the comonomer. The incorporation of a comonomer generally makes the packing of a chain into the crystalline arrays more difficult because the comonomer, with its different shape, cannot fit into the crystallite. As the thermodynamic equilibrium is approached, the decrease in T_m can be expressed as[83]

$$T_{m(\text{copolymer})} \approx \frac{1}{T_{m(\text{homopolymer})}} - \left(\frac{R \cdot \ln(1-m)}{\Delta H_f}\right) \tag{3}$$

where m is the mole fraction of the comonomer in a random copolymer. Equation (3) can also be applied to polypropylene homopolymer if the stereochemically distinct sequences of monomers (meso and racemo diads, triads, etc.) are considered as comonomers.[84, 85, 86]

The dependence of the melting temperature on the isotacticity of polypropylene has been well documented.[84, 86, 87] According to the *exclusion* model, described by equation (3), the dependence is due to the exclusion of the stereoerrors from the crystalline lamellae, which leads to a decrease in the lamellar thickness and, according to equation

(2), to a decrease of the melting temperature. Hauser et al.[88] argue, however, that the effects of comonomer and l_c are separate, but additive. The same dependence of T_m on the isotacticity of polypropylene can also be described with the defect *inclusion* model.[89] According to this model, the change in melting temperature is due to the change in the values of T_m^0 and ΔH_f^0. In the *exclusion* model these parameters are constant, but in the *inclusion* model the incorporation of the comonomer (stereoerrors) in the crystal lattice changes the unit cell parameters, which leads to the dependence of T_m^0, ΔH_f^0 and σ_f on isotacticity. Cheng et al.[86] determined the unit cell parameters for iPP fractions with isotacticity ranging from 78.7% to 98.8% and concluded that defects are included in the iPP lamellae and that the *inclusion* model can be used to describe the extrapolated equilibrium data. The inclusion of defects was found to depend on T_c and isotacticity. With higher isotacticity and T_c the defects are more concentrated in the amorphous layer.[90]

The determination of the parameters of equation (2) has proven to be difficult. For T_m^0 of iPP, the determined values range between 152 and 220 °C.[84] Bicerano[84] estimated from literature values that the ultimate value ($T_m^{0,ult}$) lies between 196.5 and 220 °C. Iijima et al.[91] concluded on the basis of their SAXS and DSC measurements that the correct value (T_m^0(perfect)) is in the range between 187 and 194 °C. The most recent result is from Yamada et al.,[92] who obtained a value of 186.2 °C with iPP having *mmmm-%* equal to 99.6. The effects of heating rate (β) and lamellar thickening (of thin lamellae) on T_m were accounted for in the determination of this value.

As mentioned above, the lamellar thickness strongly depends on T_c. The dependence of l_c on isotacticity is very weak, however.[84, 91] With increasing isotacticity and fixed T_c, l_c increases only slightly. This result is in agreement with the crystallisation model proposed by Strobl,[81] because of the initial formation of the less constrained crystal phase in this model.

3.2.4 Tacticity Distribution

The distribution of the stereoerrors in polypropylene can vary both inter- and intra-molecularly. Intermolecular variation involves the distribution of the stereoerrors in a single chain, which originates from the characteristic behaviour of the active site, while the latter involves the distribution among chains, which originates from active sites with different stereospecificities. Clearly, both of these distributions can have a marked effect on the mechanical properties of the material.[87] Fractionation of the polymer is necessary for analysis of the tacticity distribution. This can be done by extraction with a series of solvents, solvent–non-solvent pairs or series of solvents with increasing temperature.[93, 94, 95, 96, 97] Another category of fractionation methods is based on controlled crystallisation of the sample. This group comprises methods such as TREF (temperature rising elution fractionation)[98, 99], Crystaf[100] and the calorimetric thermal fractionation methods SIST (stepwise isothermal segregation technique)[101, 102] and SSA

(successive self-nucleation and annealing).[103] The advantage of the controlled crystallisation methods is the significantly easier operation. Although TREF, and the other crystallisation methods, were originally developed for the analysis of polyethylene and ethene copolymers,[98, 99] they have since been applied for polypropylene[87, 104] and random copolyester[105, 106] to obtain qualitative information about the chemical composition.

For copolyesters it has been observed that the fractionation mechanism in TREF is based on the longest crystallisable sequence.[105, 106] The longest sequences not interrupted by branching points or by comonomers that cannot enter the lamellar structure determine the highest crystallisation temperature of a chain. When the temperature is lowered during the crystallisation phase in TREF, the chains with the longest sequences are the first to form thermodynamically stable crystals and segregate. Upon further lowering of the temperature, a second layer, formed of chains with second longest crystallisable sequences, forms on top of the first crystallites. The third and following layers are formed in similar fashion. According to this scheme, the distribution of the regular sequences along the chain does not influence the fractionation. TREF gives information only about the inter-chain distribution of the longest crystallisable sequence. Applied to polypropylene, this means that the distribution of the longest isotactic sequence is determined. The results of Viville et al.[87] suggest that this is indeed the case for PP. According to Beigzadeh et al.,[107] the fractionation of polyethylene-1-octene copolymers in Crystaf is likewise based on the longest crystallisable sequence of the chain.

In the calorimetric thermal fractionation methods, analysis is based on the melting behaviour of the samples after controlled crystallisation. For best results, Wild et al.[108] used solution crystallisation, but similar results can be obtained with pure samples and controlled thermal treatments, such as SIST and SSA. If the molecular segregation during the crystallisation is successful, the remaining difference between the melting curve and the TREF fractogram is due to the dependence of the heat capacity C_p on crystallinity. Because of this, the melting curve is not mass dependent like the corresponding TREF fractogram, and an additional calibration has to be applied.[108]

The advantage of DSC methods, besides the shorter measurement times, is the additional information that is obtained on the polymer structure. If shorter sequences along the chain have crystallised, they will contribute to the melting curve.[109] With calorimetric methods, therefore, it is in principle possible to get information on the intra-molecular distribution of crystallisable sequences.

4 Experimental

Details of the experiments can be found in the original publications I-IV. Only summaries are given here.

4.1 Computational Details

All density functional theory (DFT) calculations presented in publication II were carried out with the DMol[3] program versions 4.0 and 4.2 (Accelrys Inc.).[110] The geometries were optimised using non-local DFT with Becke's exchange functional[111] and the Lee-Yang-Parr correlation functional[112] (BLYP). Owing to the small size of the $TiMg_2Cl_6$ cluster, the Cl-Ti-Cl angles were constrained to 90° and the rings were held planar in all geometry optimisations. Double numeric basis sets augmented with polarization functions (DNP)[110] were used in all calculations. In view of the expected agostic interactions, polarisation functions were also used for hydrogens. Because of the paramagnetism of the system the unrestricted method was used. The SCF convergence criterion was 10^{-7} Hartrees.

4.2 Materials

Details of the preparation of the polypropylene samples examined in studies I, III and IV are given in the respective papers. All samples were prepared at the R&D research centre of Borealis Polymers Oy in Porvoo, Finland. Polymerisations were laboratory-scale batch polymerisations. A proprietary catalyst of Borealis Polymers Oy (4^{th} generation Ziegler-Natta catalyst (see publication I)) was used.

4.3 Fractionation and Characterisation

Fractionation of the polypropylene samples is described in publication III. Briefly, the samples were fractionated with a series of solvents of increasing boiling points at increasing temperatures. Polypropylene materials were characterised by size exclusion chromatography (SEC), ^{13}C NMR, temperature rising elution fractionation (TREF) and differential scanning calorimetry (DSC). Details are given in the original publications I, III, IV.

4.4 Propagation Models

A program was written to fit statistical propagation models to the ^{13}C NMR data[III] of the polypropylene fractions. The algorithm in the program is based on the matrix multiplication technique.[66, 113] The advantage of this method is that the complex set of equations that describes the probabilities of occurrences of the steric diads, triads, etc. (*m, r, mm, rm, rr, ...*) can be represented with use of concise stochastic matrices. By way of example, the matrix **A** for the EsCE model is shown below. P_{12} and P_{21} are the

probabilities for switching from site control to chain-end control and *vice versa*, respectively. S and R are the configurations of the last-inserted (rows) and the new (columns) monomer unit.

Es/CE =

	R	**S**	**R**	**S**
R	$(1-P_{12})(\sigma)$	$(1-P_{12})(1-\sigma)$	$P_{12}(P_m)$	$P_{12}(1-P_m)$
S	$(1-P_{12})(\sigma)$	$(1-P_{12})(1-\sigma)$	$P_{12}(1-P_m)$	$P_{12}(P_m)$
R	$P_{21}(\sigma)$	$P_{21}(1-\sigma)$	$(1-P_{21})(P_m)$	$(1-P_{21})(1-P_m)$
S	$P_{21}(\sigma)$	$P_{21}(1-\sigma)$	$(1-P_{21})(1-P_m)$	$(1-P_{21})(P_m)$

In short, the fractional abundance of a stereosequence is given by

$$\mathbf{f}(d_1 d_2 ... d_n) = \mathbf{f}_0^{\mathrm{T}} \mathbf{A}_1 \mathbf{A}_2 ... \mathbf{A}_n \mathbf{J}$$

where d_k is *r* for racemo diads and *m* for meso diads, $\mathbf{J} = |111...|^{\mathrm{T}}$ and $\mathbf{A}_k$ is $\mathbf{A}_r$ when $d_k=r$ and $\mathbf{A}_m$ when $d_i=m$. $\mathbf{A}_k$ is obtained by setting elements (P_{ij}) of the matrix with $i+j$ odd to zero for $\mathbf{A}_m$ and elements with $i+j$ even to zero for $\mathbf{A}_r$. $\mathbf{f}_0^{\mathrm{T}}$ is the vector of the stationary probabilities which can be solved by evaluating the equations $\mathbf{f}_0^{\mathrm{T}}\mathbf{A} = \mathbf{f}_0^{\mathrm{T}}$.[65]

The model parameters were optimised with Simplex[114] and DONLP2[115] algorithms using a least-squares method.

$$\chi^2 = \sum_k \sum_j (I_{\mathrm{exp},j,k} - I_{calc,j,k})^2$$

$$I_{calc,j,k} = \sum_i w_{ik} I_{ijk}$$

$I_{calc,j,k}$ is the calculated total intensity for stereosequence *j* in fraction *k*. w_{ik} is the weight fraction of the component *i* in fraction *k* and I_{ijk} is the calculated intensity for sequence *j* with component *i* and fraction *k*. $I_{exp,j,k}$ is the experimental intensity for sequence *j* in fraction k.

A new approach was applied for comparison of the propagation models. A program was written to generate a set of chains with the parameters obtained from the fit. A similar approach has previously been used in the evaluation of Crystaf data for polyethylene-1-octene copolymers.[107] From the results of this program, the weight fractions of the chains with a given longest crystallisable sequence were obtained. This result is presented as a curve of weight fraction vs. temperature. The melting temperature is approximated from the sequence length using equation 2. Altogether 200 000 chains were generated in each run. Two different termination probabilities (P_{tr}) were used: 0.01 and 0.001.

5 Main Results and Discussion

A summary of the results reported in publications I-IV is presented in the following. Some unpublished data are included.

5.1 Regioselectivity of the Polymerisation Reaction[II]

The mechanism of the polymerisation reactions and the regiospecificity in propene polymerisation were studied by performing density functional theory calculations on a model catalyst site. The calculations were performed in order to study and verify the formation of a dormant site after 2,1 insertion. The investigation is reported in detail in publication II.

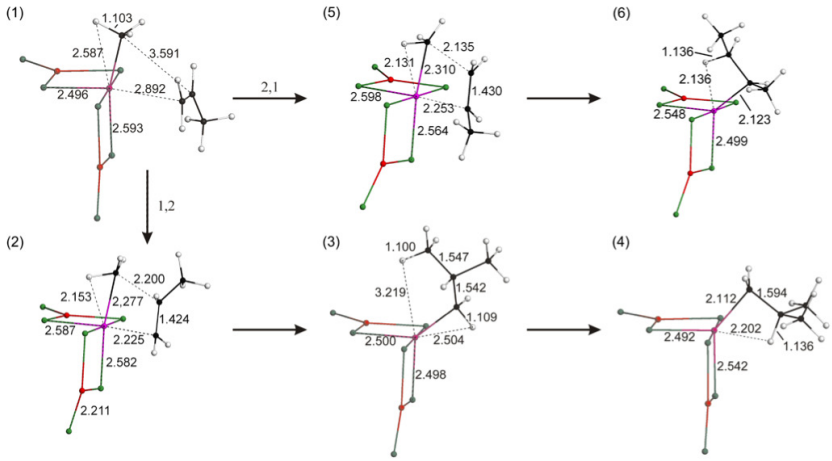

Figure 5 *First insertion reactions.*[II]

5.1.1 First Insertions

Figure 5 shows the 1,2 and 2,1 propene insertion reactions at the model active site. In both reactions, the polymerisation reaction proceeds through a four-member transition state. After the transition state **2** in the 1,2 insertion, the product **3** is formed with an energy gain of 9.9 kcal/mol (41.4 kJ/mol). The stretched C–H bond indicates that this conformation is stabilised by an α-agostic interaction (C_α-H_α = 1.109 Å). Rotation of the C_α-C_β bond by 60 degrees brings the β-hydrogen close to the titanium. Optimisation of this structure yields the final product **4** of this insertion reaction with an energy gain of 11.7 kcal/mol (49.0 kJ/mol). These results are in line with experimental estimates (9.5–12.0 kcal/mol (39.8–50.2 kJ/mol))[116, 117] and close to the values obtained by Boero et al.[52] with the stereospecific 5-fold site in the second insertion (activation energy 10.8 kcal/mol (45.2 kJ/mol) and final energy gain 16.7 kcal/mol (69.9 kJ/mol)).

The corresponding 2,1 addition was simulated starting from the same π-complex **1** and the reaction proceeded similarly to the 1,2 insertion. The activation energy was 2.8 kcal/mol (11.7 kJ/mol) higher and the transition state **5** was formed at a slightly shorter distance of 2.14 Å. The product **6** is directly formed in the β-agostic conformation, however, and the energy gain is 2.3 kcal/mol (9.6 kJ/mol) lower than in the 1,2 insertion.

5.1.2 Second Insertions

The relative probability of further insertions to the two sites **4** and **6** determines whether the 2,1 insertion results in a dormant site for polymerisation.

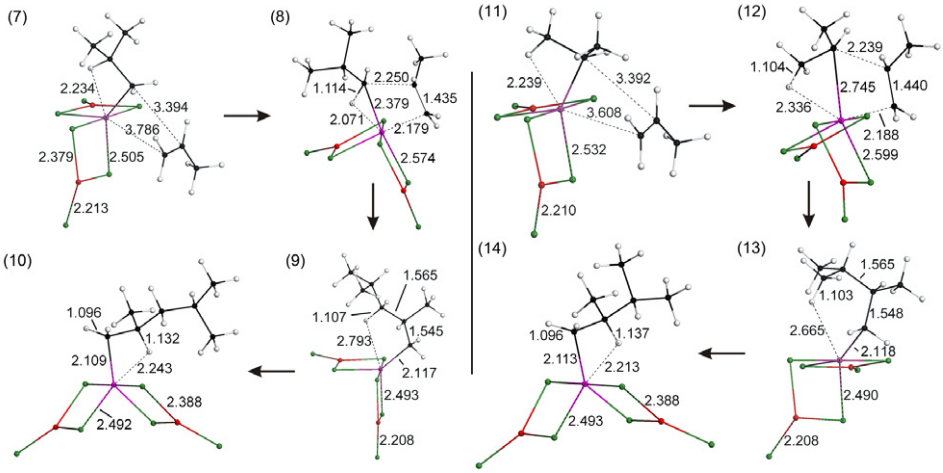

Figure 6 *Second insertion reactions.*[II]

The determination of the reaction energies was more complex for these reactions than for the first insertions. For ethene, Cavallo et al.[21] report a barrierless insertion to the β-agostic ethyl complex with the same model catalyst site (structure 10 in ref. 21). In the present case, with propene, a stable π-complex could not be found. Every time an optimisation was performed with propene placed near the active site, the result was the migration of propene away from the catalyst model. The same occurred with the site containing 2-methylpropyl, even when the Ti-C_1 distance was initially constrained. Also in the present case, a stable π-complex was obtained with ethene.[II]

Figure 6 shows the calculated second 1,2 insertion reactions. The calculations were started with propene about 3.7 Å away from Ti. Even though a stable π-complex was not obtained, the basic mechanism of these reactions was similar to that of the first insertions: the propene double bond aligns itself parallel to the Ti-C_α bond and the four-member transition state is formed at C_α-C_1 distance of 2.24–2.25 Å (Figure 6). Because

the starting structures are β-agostic, however, there are also differences. Figure 7 shows the evolution of the relevant distances between atoms as a function of the reaction coordinate.

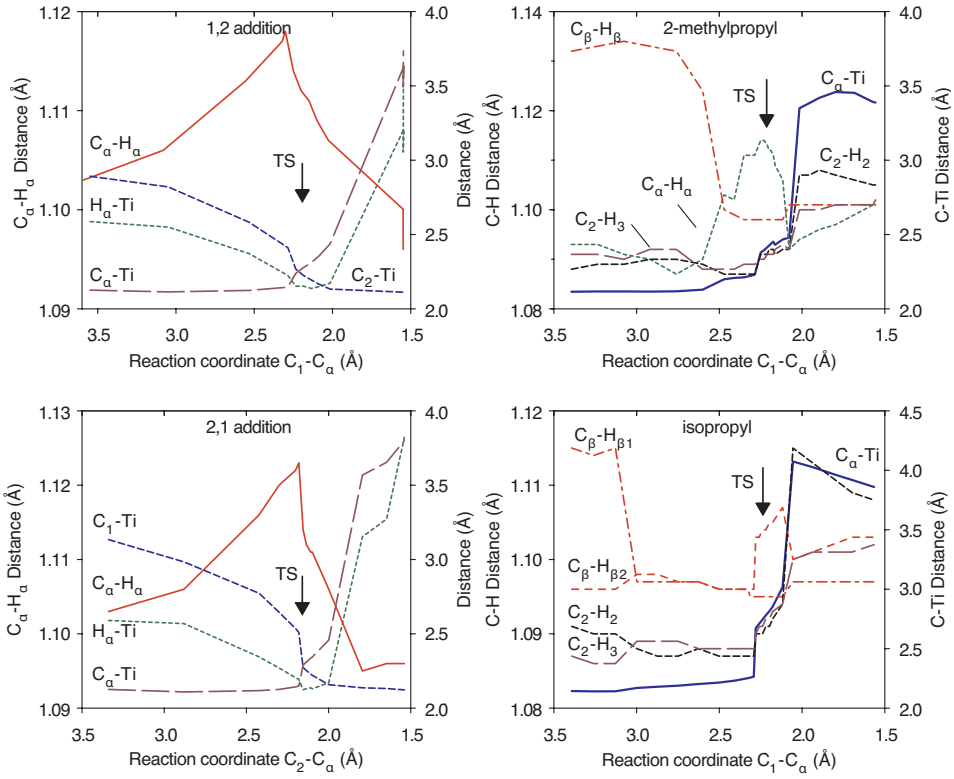

Figure 7 *Some relevant changes in distance during the first 1,2 and 2,1 insertions (left side) and insertions to the sites containing 2-methylpropyl and isopropyl group (right side). Transition states are marked with an arrow.*[II]

In the first insertions (Figure 7, left side), the facilitating agostic interactions are clearly seen in the C_α-H_α distances (solid lines), which pass through a maximum before the transition state. In the second insertions (Figure 7, right side), the strong β-agostic interaction is seen at the start of the reaction. In the case of the 2-methylpropyl site the β-agostic interaction starts to break at a C_α-C_1 distance of about 2.6 Å, and in the case of the isopropyl site the interaction vanishes already at a C_α-C_1 distance of 3.0 Å. For both insertions there is a small agostic stabilisation near the transition state, but it is clearly weaker than in the first insertions. In the case of the 2-methylpropyl group, the interaction is α-agostic due to the rotation of the chain around the Ti-C_α bond as the C_α-C_1 distance is shortened. For the transition state **12**, the stabilisation is due to a much weaker β-agostic interaction.

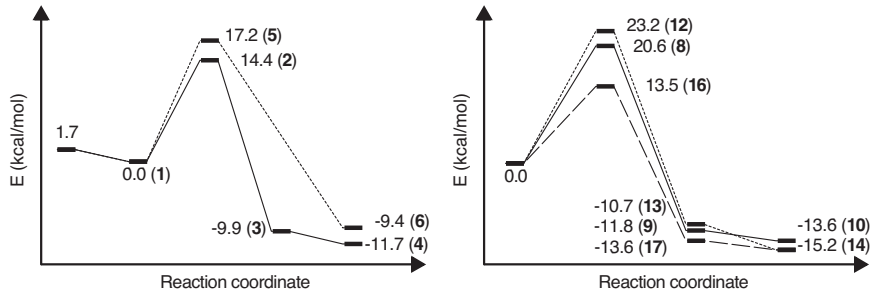

Figure 8 *Energy diagram of the first and second insertion reactions. Number of the corresponding structure in parenthesis.*[II]

The energies of the reactions are summarised in Figure 8. As expected, in the first insertions the 1,2 insertion is preferred. The difference between the activation energies of 1,2 and 2,1 insertions is 2.8 kcal/mol (11.7 kJ/mol). Also the second insertion is preferred to this site (2.6 kcal/mol (10.9 kJ/mol)). Although these results show that the addition after 1,2 insertion is preferred, the activation energies of the second insertions (20.6 (86.2) and 23.2 (97.1) kcal/mol (kJ/mol)) were surprisingly high relative to the first insertions and to the experimental estimates (9.5–12.0 kcal/mol (39.8–50.2 kJ/mol)).[116, 117]

This result together with the lack of stable π-complexes suggests that the calculated paths may not be the preferred reaction paths. With the 5-fold site, Boero et al.[52] found that the activation energy for the second insertion is comparable to that for the first insertion (10.5 kcal/mol (44.0 kJ/mol)). In their case, also the second insertion was α-agostic assisted because the rotation of the chain to β-agostic state was not barrierless.

5.1.3 Conversion from α- to β-agostic Structure

Further calculations were performed to investigate the energetics of the conversion between the α-agostic and β-agostic states and the energetics of the second insertion to an α-agostic isopropyl site. Figure 9 shows the calculated insertion reaction, which was started from the stable π-complex **15**. The activation energy for this reaction was 13.5 kcal/mol (56.5 kJ/mol) **16**, which is lower than the first insertion activation energies by 0.9–3.7 kcal/mol (3.8–15.5 kJ/mol). The final energy gain was 3.5–5.6 kcal/mol (14.7–23.4 kJ/mol) higher than in the first insertions.[II]

Because the insertion to the isopropyl site from an α-agostic π-complex is of comparable energy to that of the first insertions, the rate-determining step for insertion must be the formation of the π-complex. In the case of the β-agostic structure, this requires a conversion to an α-agostic structure.

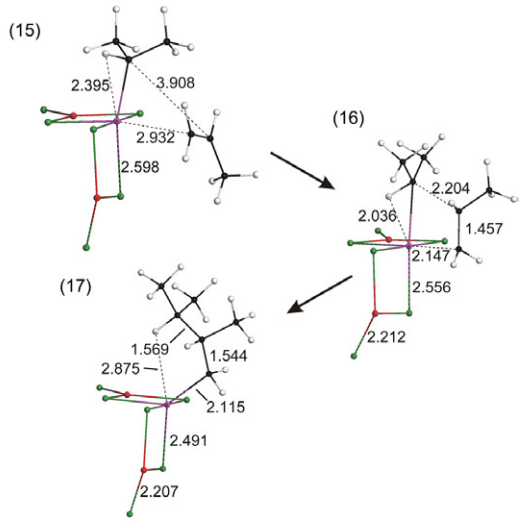

Figure 9 *1,2 Insertion to an α-agostic isopropyl site.*[II]

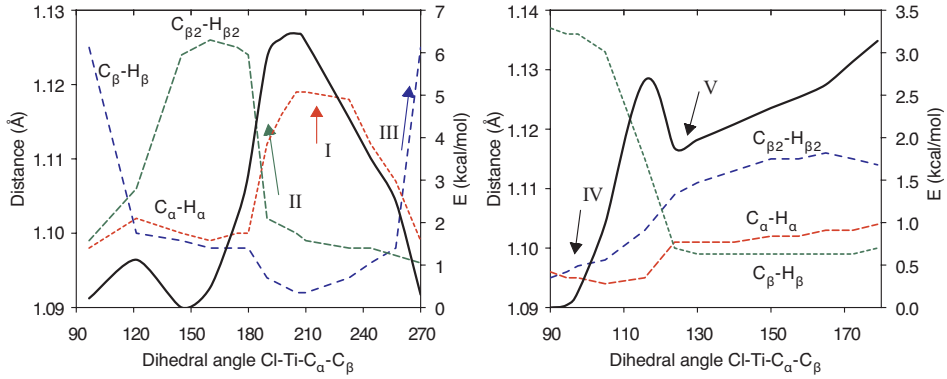

Figure 10 *Energy diagram for the rotation of the dihedral angle Cl-Ti-C_α-C_β (solid line) and relevant changes in distance (dashed lines) at the site containing isopropyl group (left side) and the site containing 2-methylpropyl group (right side). Left side: stretching of the bonds caused by α- and β-agostic interactions is marked with arrows (I and II, III, respectively). Right side: α- and β-agostic minimum energy conformations are marked with arrows (V and IV, respectively).*

Figure 10 shows the calculated energy diagrams for the torsion of the dihedral angle Cl-Ti-C_α-C_β for isopropyl (left) and 2-methylpropyl (right) sites. Owing to the symmetries of the systems, only 180° and 90°, respectively, are shown. For the isopropyl site, the energy diagram (solid line) shows three β-agostic minima, while for the 2-methylpropyl site it shows one β-agostic and one α-agostic minimum. In the case of the isopropyl site there is a clear stretching of the α-hydrogen bond (arrow I), which indicates an agostic interaction, but the stronger β-agostic interactions render this an energy maximum

instead of a minimum. The result of the missing minimum was already seen in the 2,1 insertion reaction, in which the product was formed directly in the β-agostic state.

According to these results, the 1,2 insertion to the site containing the isopropyl chain is disfavoured by over 5 kcal/mol (20.9 kJ/mol). The limiting step is the formation of the π-complex, which can only form with the α-agostic state. After a 1,2 insertion, the chain is initially formed in the α-agostic state, and even though it is not the global minimum the rotation barrier is not very high. After a 2,1 insertion, the chain will rotate directly to the β-agostic state. Insertion to this site requires a concerted rotation of the chain and a monomer attack. Although this kind of reaction is highly unlikely, it allows one to hypothesise that an increase in the monomer concentration will increase regioerrors in atactic polymer chains.

The mechanism found in this study is markedly different from that found for the *rac*-$Me_2C(3\text{-}t\text{-Bu-1-Ind})_2ZrCl_2$/MAO homogeneous catalytic system.[118] In that system, isopropyl blocked the active site with a conformation that had a double β-agostic interaction with the metal. This kind of interaction was not found in the present system.

An interesting observation is that ethene, but not propene, is able to form a stable π-complex with the site containing a β-agostic chain. This explains the experimental finding that ethene reversibly enhances the rate of propene polymerisation and that hydrogen does not activate ethene polymerisation.[119]

5.2 Effect of Al/ED Ratio on the Polymer Structure[I]

The effect of the electron donors on the polymer structure was studied by performing a series of polymerisations with different Al/ED (Al/D_2 in publication I) ratios and characterising the resulting polymer structures. The results were interpreted using a model of the active sites based on an equilibrium reaction between the catalyst and the electron donor.[I] The series of polymerisations and the analytical results are listed in Table 2.

Table 2 and Figure 11 show the average activities obtained in the test series measured as kg PP/g cat.h. The average activity of the polymerisation increased at the beginning of the series from 31.6 to 44.3 kg PP/g cat.h when the ED/Ti molar ratio was increased from 2.5 to 10. At still higher ED/Ti molar ratios, a gradual decrease in the average activity could be observed. Thus, the activity decreased to about 28 kg PP/g cat.h when the ED/Ti molar ratio was increased from 10 to 83.

Table 2 Polymerisation conditions and changes in the polymer structure in the test series.[I]

Sample	Al/ED	ED/Ti	Activity	XS	Isotacticity ^{13}C NMR	MFR	$\overline{M_n}\cdot 10^3$	$\overline{M_w}/\overline{M_n}$
	mol/mol	mol/mol	Kg PP/g cat.h	wt.-%	*mmmm*-%	g/10 min		
1	100	2.5	31.6	4.1	94.58	12.2	35.9	7.9
2	80	3.1	31.7	2.7	95.04	8.6	41.9	7.1
3	50	5	40.9	2.0	96.38	6.8	49.1	6.2
4	25	10	44.3	1.4	-	5.5	-	-
5	10	25	41.3	1.0	97.20	4.8	50.5	6.5
6	3	83	27.5	0.8	98.10	5.3	57.5	5.6

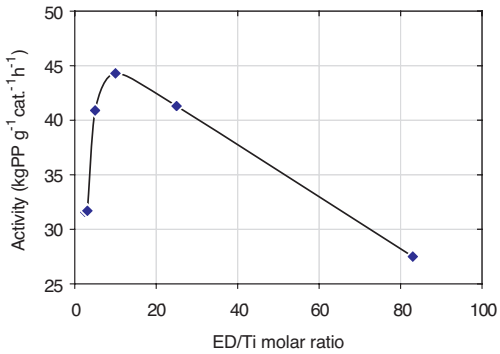

Figure 11 *Influence of the ED/Ti molar ratio on the average polymerisation activity.*[I]

The isotacticity (measured by ^{13}C NMR) in the test series increased up to the ED/Ti ratio of 5. A corresponding decrease occurred in the amount of "atactic" xylene-soluble fraction (XS) (Table 2 and Figure 12). Further increase of the ED/Ti ratio resulted in only a minor change. These results correlate well with the activity results, as most of the change in isotacticity took place between the ED/Ti molar ratios 2.5 and 10. Figure 12 shows the melt flow rate (MFR) and number average molar mass $\overline{M_n}$ as function of the ED/Ti molar ratio. Comparison of the graphs in Figure 12 reveals another correlation in the test series, between the changes in molar mass and isotacticity. In $\overline{M_n}$, as in isotacticity, the largest increase occurs below ED/Ti ratio 5. At higher ED/Ti ratios the change is much slower. The melt flow rate, which is known to decrease with increasing molar mass, shows an opposite trend.

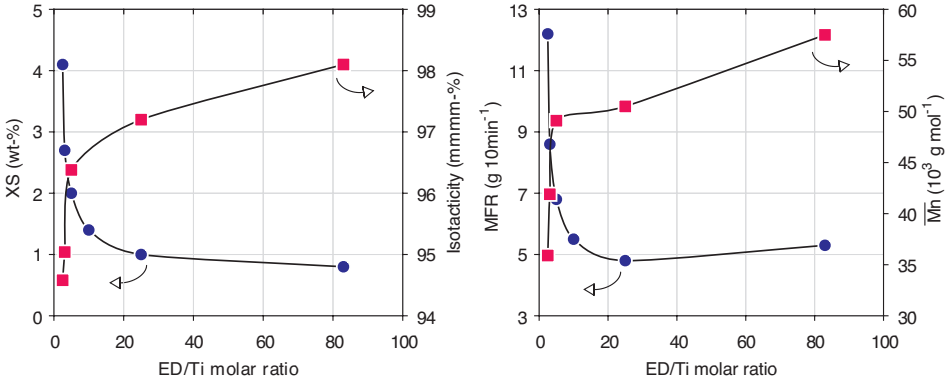

Figure 12 *Left: influence of the ED/Ti molar ratio on the isotacticity measured by NMR and on the xylene soluble fraction (XS). Right: influence of the ED/Ti molar ratio on the melt flow rate (MFR) and* $\overline{M}_n$*.*[I]

In the model of the active sites,[I] the change in the activity in the test series can be understood as an increased complexation of the external donor with the catalyst and, hence, as a decrease in the number of donor-free sites. According to Chadwick et al.,[120] stereoirregular and regioirregular monomer insertions result in a dormant site. Their finding is also supported by the results of our calculations with a model catalyst site.[II] The irregular insertions are much more frequent in donor-free sites. The deactivation with a high ED/Ti ratio is more difficult to rationalise.[I]

The changes in both isotacticity and molar mass can be explained with the presented equilibrium of the electron donor coordinated to either the catalyst or the cocatalyst (reaction (1) in I). An increase in isotacticity is expected with an increase in the amount of donor because the equilibrium is shifted to the right, i.e. towards isotactic polymerisation. According to the fractionation studies, the part of polypropylene with low isotacticity also has low molar mass.[121, III] This explains the observed increase in the molar mass as well. It seems that the donor-free sites produce polymer with lower $\overline{M_n}$.[I]

The suggested equilibrium reaction also affects the lengths of the isotactic sequences. A change in the balance of the equilibrium reaction should result in an increase in the lengths of the isotactic sequences in the test series. Figure 13 shows the sequence length distributions calculated from SIST curves.[I] The results indicate that there is an increase in the populations containing longer isotactic sequences (>87) when more donor is used in the polymerisation. Correspondingly the populations of shorter sequences are decreased.

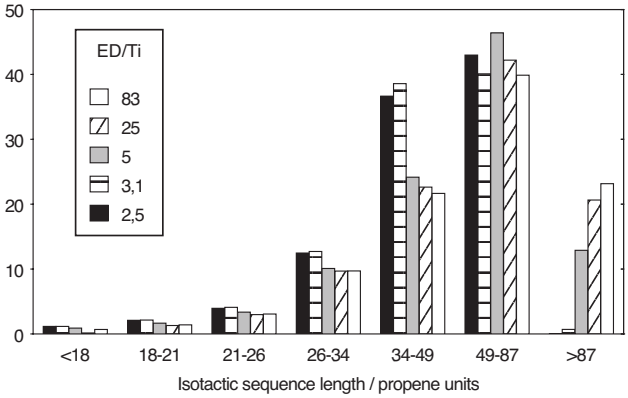

Figure 13 *Influence of the ED/Ti molar ratio on the distribution of isotactic sequence lengths in the polymers. (Sequence length intervals correspond to 10 °C in temperature.)*[I]

5.3 Solvent Fractionation and SSA Measurements[III, IV]

Applicability of the successive self-nucleation and annealing (SSA) DSC method for analysis of the tacticity distribution in polypropylene was investigated with two polypropylene samples. The samples were prepared with different Al/ED ratios in order to obtain one sample with high isotacticity and another with low. The samples were fractionated by using a series of hydrocarbon solvents of increasing solvent power. The details of the fractionation are presented in publication III and the SSA measurements in publication IV.

Table 3 *Results from the solvent fractionation of two polypropylene samples (A and B) and from thermal analysis of the fractions.*[III]

Sample			**A**			**B**		
Fraction	Solvent	Temp. (°C)	Weight-%	T_m (°C)	Cryst. (%)	Weight-%	T_m (°C)	Cryst. (%)
1	pentane	25				10.0	-	-
2	pentane	35				1.7	107.8	12.8
3	hexane	45				3.0	123.4	25.2
4	hexane	60				0.2	128.4	28.7
5	octane	80	1.2	124.7	22.1	0.3	136.6	26.6
6	toluene	75	0.1	137.0	34.6	0.4	159.6	26.8
7	toluene	94	2.2	149.5	51.9	27.4	156.3	46.2
8	xylene	112	70.4	163.8	52.8	52.6	161.2	47.7
9	xylene	127	26.3	165.2	49.8	2.7	161.4	48.5

Table 3 lists the solvents and temperatures used in each fractionation step, along with the fractionation results and the results of the DSC analysis of the polypropylene fractions. From the melting temperatures and crystallinities it is evident that the fractionation proceeded mainly according to the stereoregularity. Fractions of the two

samples extracted with the same solvent at the same temperature, however, have different isotacticities, which indicates that the controlling factor in the fractionation is not the average isotacticity but the lengths of the crystallisable isotactic sequences in the chains.[III] The fractionation thus resembles that achieved with TREF,[87] and the resemblance is also seen if the weight fractions (wt.-%) are compared with analytical TREF fractograms of the samples (Figure 14). Like the isotacticities, also the molar masses increase in the last fractions (Figure 15). As reported earlier, the isotacticity and molar mass correlate in polypropylene prepared with Z-N catalyst.[I]

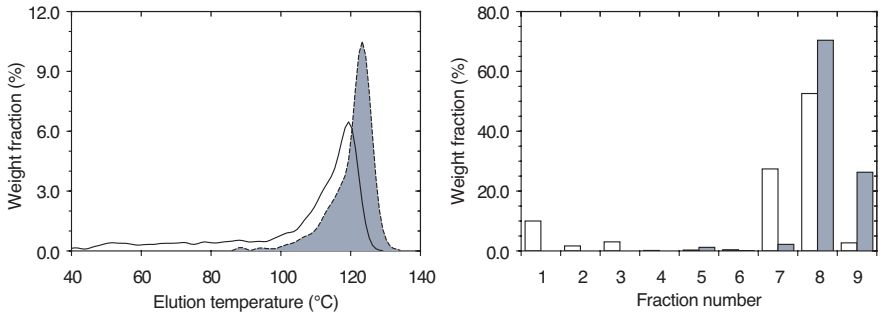

Figure 14 *TREF fractograms of the polypropylene samples A and B (left side) and weight fractions of the obtained polypropylene fractions of samples A and B (right side).*[III]

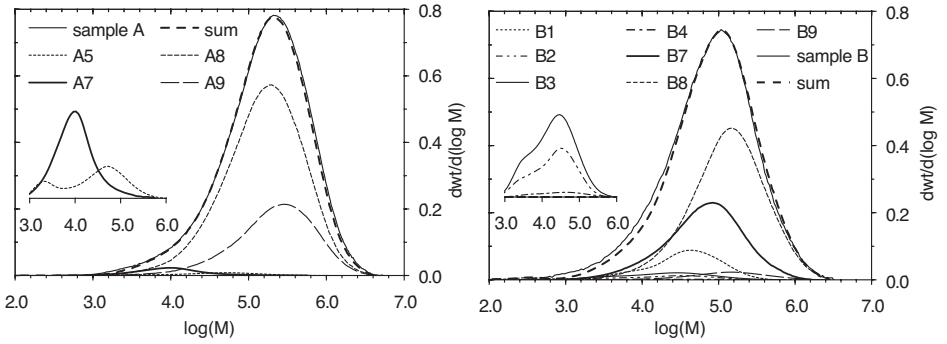

Figure 15 *Molar mass distributions of samples A and B with the weighted distributions of the fractions and their sum. Distributions of the smaller fractions (A5, A7 and B2-B4) are shown on the left at magnified scale.*[III]

With respect to the effect of the electron donor in the polymerisations of the samples A and B, it is clear that the site responsible for the atactic material is deactivated almost completely by the external electron donor. In addition, both the molar mass and isotacticity of the isotactic fractions increase and their distributions become narrower. The 15-fold decrease of the octane-soluble fraction is a combined outcome of these

effects. These observations are in good agreement with the model based on the equilibrium reaction.[I]

5.3.1 SSA Thermograms

The SSA melting curves of the fractions are shown in Figure 16. The lower melting fractions show broad thermograms with multiple melting peaks, representing the material that has crystallised in the successive steps of SSA. The endotherms of the more isotactic fractions are narrower and contain only one or two clear peaks. The heating rate in these measurements was 10 K/min. With a lower heating rate, multiple melting peaks are also observed in the more isotactic fractions (Figure 17). According to Yamada et al.,[92] melting kinetics influences the observed melting peak value. They found that equation (4) can be used to describe the change in melting peak as a function of the heating rate (β).

$$\delta T_m = 3.7 \cdot \beta^{0.2} \tag{4}$$

As shown in Figure 17 (right), the equation fits well the values extracted from the SSA melting peaks for sample A[IV]. The good fit indicates that lamellar thickening has not occurred during the heating of sample A. Lamellar thickening does occur in the lower melting fractions but it is significant only at low heating rates (β < 10 K/min) (fraction B4 in Figure 17)

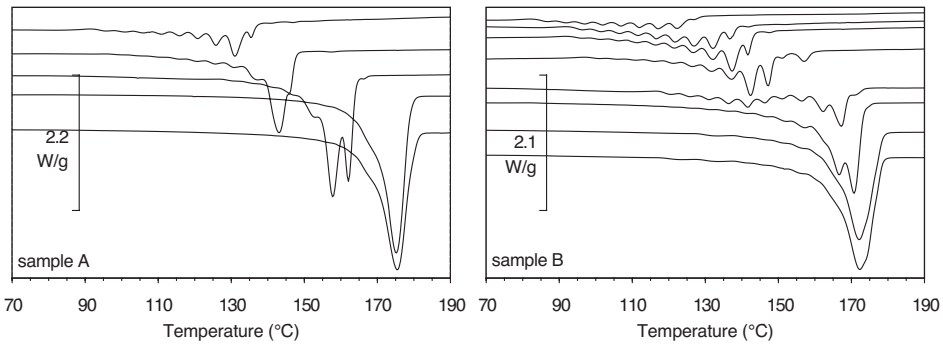

Figure 16 *SSA melting curves of the polypropylene fractions. Order of the curves from top to bottom: sample A 5-9 and sample B 2-9.*[IV]

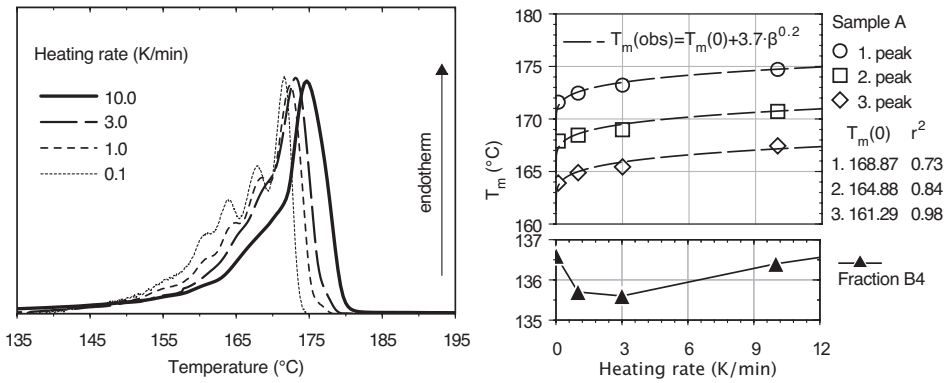

Figure 17 *On the left, effect of heating rate on the SSA melting curve of polypropylene (sample A in IV). On the right, SSA melting peaks as a function of the heating rate for sample A and fraction B4.*

Figure 18 shows the weighted version of the SSA melting curves for the fractions shown in Figure 16 along with the SSA melting curves of the original sample. Good correspondence between the melting curve of the original sample and the sum curve of the fractions indicates that the measurement is quantitative for a broad range of tacticities.

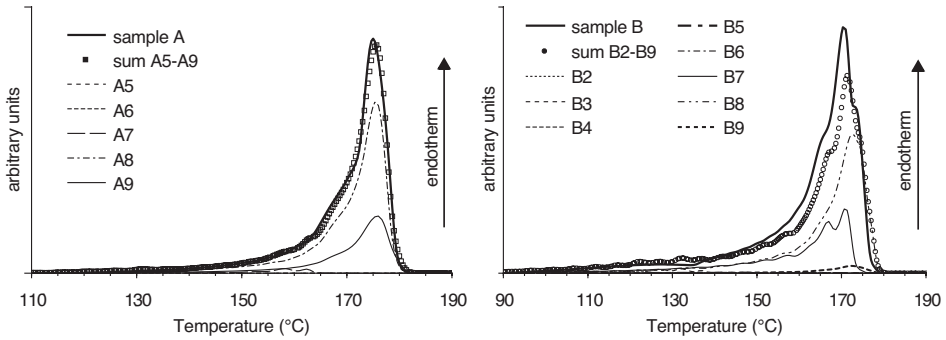

Figure 18 *Weighted SSA melting curves of the fractions and the SSA melting curves of the original samples A (left) and B (right).*

5.3.2 Comparison of SSA and TREF measurements

According to literature results,[87, 105, 106] the segregation in TREF is based on the longest crystallisable sequence. According to Gabriel et al.,[122] calorimetric thermal fractionation also gives information about the intramolecular chemical composition distribution of the polymers. It was not expected, therefore, that SSA and TREF would yield the almost identical results seen in the curves of Figure 19. From these results, it was concluded[IV] that SSA and TREF give very similar information. As shown in Figure 17, the melting

curve depends on the heating rate: with lower heating rate the amount of lower melting material becomes more pronounced. Even in this case, however, the difference between the results is not great, though it is clear that the SSA measurement is more sensitive to the shorter crystallisable sequences than is the TREF measurement.

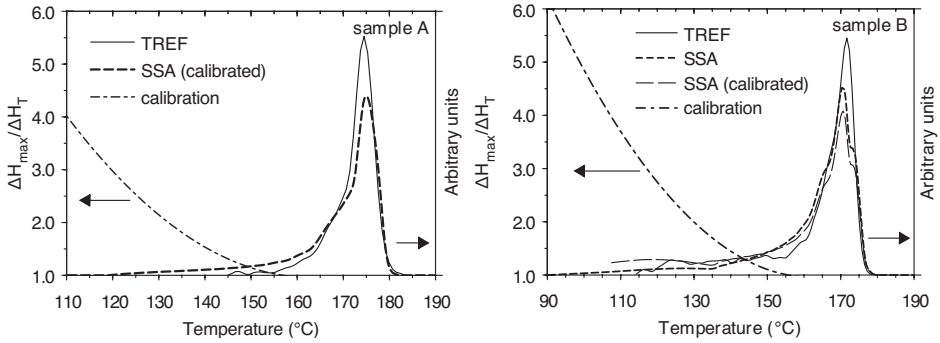

Figure 19 *Comparison of results of SSA and TREF measurements of polypropylene for sample A (left) and sample B (right).*[IV]

The difference between the SSA and TREF curves was more significant for the fractions with low isotacticities (fig 3. in IV). The TREF curve suggests that these fractions contain a bimodal distribution of tacticity, similar to their bimodal molar mass distribution (Figure 15). However, the comparison of SSA and TREF curves is more difficult for fractions with low isotacticities because the SSA melting curves are extremely broad and contain multiple peaks originating from the measurement method. In addition to this, the lamellar thickening upon heating is more significant in the thinner lamellae.[92]

5.3.3 Correlation Between Isotacticity and the SSA Results

The correlation between the polypropylene structure (stereoregularity) and the thermograms was not straightforward. The good correspondence between the SSA and TREF measurements[IV] suggested that the segregation mechanism in SSA could be similar to the one proposed for TREF. Comparison of the average isotactic sequence length (MRL) calculated from the ^{13}C NMR results and the lamellar thicknesses estimated with equation (2) suggest, however, that PP samples can be divided into three groups according to their behaviour in the SSA measurement.[IV] No correlation was found for the fraction with isotacticity over 99%. For the polypropylene fractions with narrow melting peaks and isotacticity in the range 89-99%, the lamellar thicknesses match closely with the MRL values. This result is in direct contradiction to literature reports of the segregation mechanism. On the other hand, it is in line with the *defect inclusion* crystallisation model, which according to Bicerano[85] holds for isotactic polypropylene.

In the case of samples with low isotacticities, the SSA curves are too broad to allow reliable comparisons. It is safe to assume nevertheless that the crystalline structure of these fractions is completely different from that of fractions with higher isotacticity and it is probably of fringed-micelle type.[81] Comparison of the sequence lengths and lamellar thicknesses of these fractions indicated that the longest isotactic sequences are the determining factor in the segregation. The result is easily understood since even the longest sequences are very short, and only the longest sequences are capable of crystallising.

In line with the above results, a non-linear dependence was found between the melting temperature ($T_{m,\,SSA}$) and the isotacticity of the fractions (*mm*-%) (Figure 20).

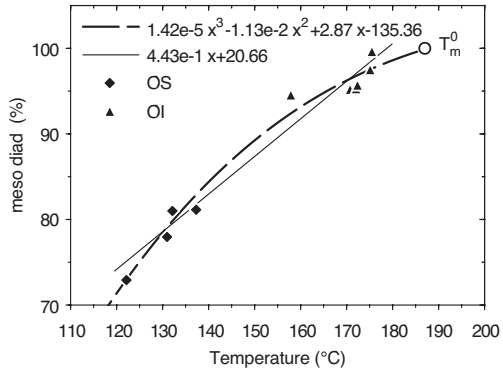

Figure 20 *mm-% values of polypropylene fractions (octane-soluble (OS) and insoluble (OI)) as a function of the SSA melting temperatures. Equilibrium melting temperature (T_m^0) shown with mm-% value of 100.0%.*[IV]

5.4 Best-fit Calculations of Stochastic Models

Figure 21 shows the fits obtained with the evaluated stochastic models. In addition to the classical two-site Es+CE model, several two-, three- and four-site models were evaluated. Moreover, for each model containing a CE component, a corresponding model with CE1 component (first-order Markovian statistics) in place of the CE component was tested. A corresponding Es1 component was not tested because it has been found to reduce to an Es component during the optimisation.[123] Of the three-site models in Figure 21, Es+C1+CE was introduced by Busico et al.[42] and Es+C1+CE1 by Randall et al.[70] All the models were fitted to the stereosequence data obtained for the fractions of the polypropylene samples designated A and B in publication III. Data with pentad/heptad level accuracy was used for the fits. The total number of sequences was 60 for sample A and 107 for sample B. In previous studies[42, 70] with the three-site models, the same components were found in the different fractions, with only the weight fractions of these components varying from fraction to fraction. In the present

case the model parameters were constrained so that the best-fit parameters represented a best-fit for this kind of model. That is, the probabilities in the models (σ, P_r, etc.) were not allowed to vary from fraction to fraction.

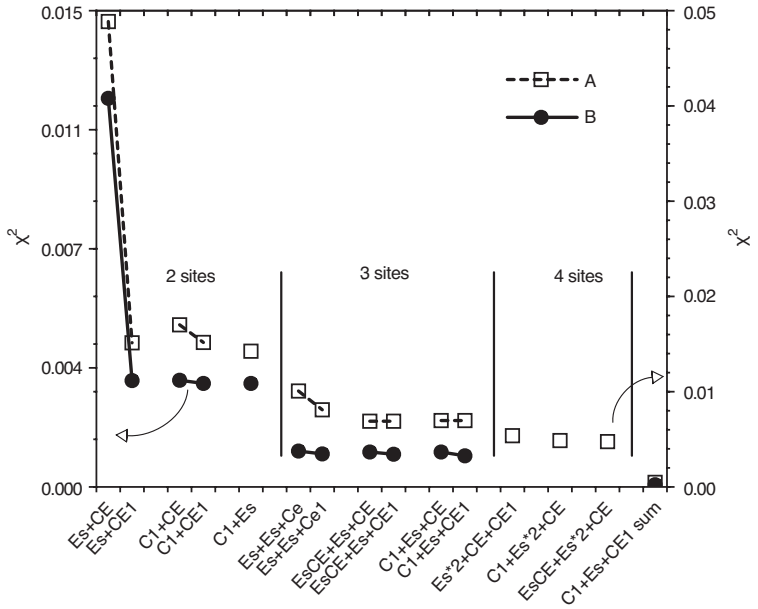

Figure 21 *The χ^2-fits of the stochastic propagation models with 2 to 4 sites to the stereosequence data of the PP fractions of samples A and B. The C1+Es+CE model was also fitted to the stereosequence data obtained by calculating the weighted sum of the fractions (C1+Es+CE1 sum).*

According to Randall et al.,[123] a CE1 component in a two-state model leads to a better prediction of the syndiotactic chains than does the CE component. In our case the Es+CE1 model gave a significantly improved fit compared to the simplest Es+CE model, with the improvement greatest in the low-melting fractions. For both A and B this model contains a highly isospecific Es component ($\sigma > 0.98$), as expected from previous studies,[41, 42, 70, 124] and a CE1 component with parameter values (P_{rr} = 0.69±0.02, P_{mm} = 0.69±0.05) similar to the ones obtained by Randall et al.[123]

The better fits in the low-melting fractions with the Es+CE1 model are mainly due to better matches with the *mmrr*-centred sequences *and mmrm+rmrr*. In the Es+CE model, *mmrr* is underestimated and *mmrm+rmrr* is greatly overestimated, while in the Es+CE1 model the remaining mismatch is due to *rrrrmm.* This is a clear indication that a "switching" component is needed to improve the fit.[125] Two different "switching" components have been used previously: EsCE and C1.[42, 70, 125] The former describes the statistics for a site that can switch between site control and chain-end control. In the

latter the change is between two diastereotopic sites (Es). P_{12} and P_{21} give the probabilities for switching from state 1 to state 2 and *vice versa*.

As shown in Figure 21, the fits with C1+CE(1) models are at the same level as fits with Es+CE1. The worse-than-expected result for a model with two additional adjustable parameters is at least partly due to the simultaneous fitting to all fractions. In the C1+CE(1) models, the CE(1) component is used to describe the high-melting fractions ($P_r \approx 0$). Though an Es+C1 model would seem more appropriate for this case, what really is needed is a three-site model. Fraction by fraction, these two-site models provide acceptable fits for the high-melting fractions, but the fits are not as good for the low-melting fractions (see Table 6).

Table 4 *Best-fit parameters for selected stochastic models.*

Es+CE(1)			**C1+CE**			**C1+Es**			**Es_1+Es_2+CE(1)**		
	A	B		A	B		A	B		A	B
σ	0.994	0.978	$\sigma_{1,1}$	0.422	0.312	$\sigma_{1,1}$	0.918	1.000	σ_1	0.860	0.770
P_r	0.494	0.623	$\sigma_{1,2}$	0.928	1.000	$\sigma_{1,2}$	0.469	0.283	σ_2	0.999	0.986
χ^2	1.224	4.886	P_{12}	0.977	0.890	P_{12}	0.743	0.717	P_r	0.826	0.883
σ	0.997	0.982	P_{21}	0.633	0.720	P_{21}	0.944	0.880	$\chi^2 \cdot 10^2$	0.113	1.007
P_{rr}	0.675	0.713	$P_{r,2}$	0.003	0.009	σ_2	0.997	0.984	σ_1	0.863	0.790
P_{mm}	0.745	0.641	$\chi^2 \cdot 10^2$	0.336	1.702	$\chi^2 \cdot 10^2$	0.326	1.425	σ_2	1.000	0.987
$\chi^2 \cdot 10^2$	0.335	1.513							P_{rr}	0.803	0.823
									P_{mm}	0.382	0.465
									$\chi^2 \cdot 10^2$	0.104	0.810

C1+Es+CE			**C1+Es+CE1**			**EsCE+Es+CE**			**EsCE+Es+CE1**		
	A	B		A	B		A	B		A	B
$\sigma_{1,1}$	0.592	0.388	$\sigma_{1,1}$	0.000	1.000	σ_1	0.989	0.840	σ_1	0.860	0.839
$\sigma_{1,2}$	0.957	1.000	$\sigma_{1,2}$	1.000	0.336	$P_{r,1}$	0.412	0.851	$P_{r,1}$	0.897	0.851
P_{12}	0.767	0.751	P_{12}	0.001	0.590	P_{12}	0.449	0.196	P_{12}	0.880	0.194
P_{21}	0.385	0.648	P_{21}	0.006	0.764	P_{21}	0.798	0.448	P_{21}	0.985	0.441
σ_2	0.998	0.985	σ_2	0.875	0.985	σ_2	0.998	0.985	σ_2	0.867	0.985
P_r	0.846	0.973	P_{rr}	0.793	0.975	$P_{r,2}$	0.841	0.996	P_{rr}	0.285	1.000
$\chi^2 \cdot 10^2$	0.110	0.697	P_{mm}	0.388	0.832	$\chi^2 \cdot 10^2$	0.110	0.690	P_{mm}	0.998	0.741
			$\chi^2 \cdot 10^2$	0.098	0.700				$\chi^2 \cdot 10^2$	0.101	0.690

Several authors have used three-site models in an attempt to obtain a better prediction of stereosequences in Z-N polypropylene. In the simplest case, one Es component is added to the classic Es+CE model.[41, 95, 124] In our work, this model provides a clearly improved fit relative to the two-site models. Again, the model with CE1 component gives a better fit. The distribution of the three components of this model in the PP fractions is shown in Figure 22. The obtained fit is in good agreement with a previous result[42] showing that Z-N PP contains highly isotactic (Es_1), poorly isotactic (or isotactoid) (Es_2) and syndiotactic (CE(1)) polypropylene. The Es+Es+CE(1) models do not, however, predict chains with a stereoblock structure. Especially in the case of fractions 3 and 4 of sample B, it is difficult to explain the high content of the syndiospecific component unless the syndiotactic and isotactoid sequences are chemically linked.[125]

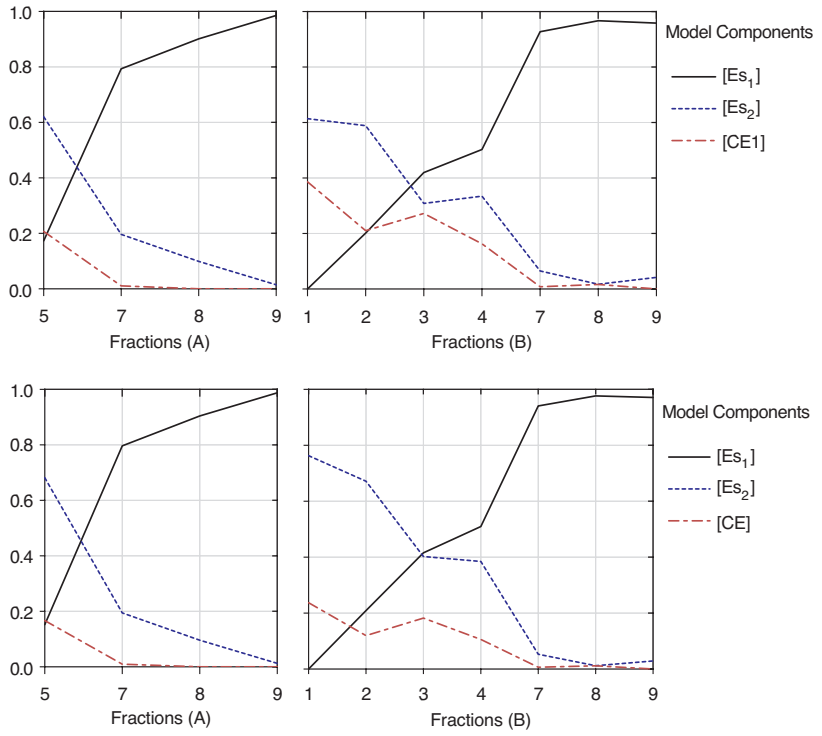

Figure 22 *Component weight fractions of the three-site Es_1+Es_2+CE(1) models for samples A and B.*

The fits obtained with the three-site models that contain a switching component are all very good. Interestingly, in the C1+Es+CE and EsCE+Es+CE models, all other parameters except the probabilities of the EsCE and C1 components are almost the same. As shown in Figure 23, the weights of these components match very closely, which means that, in these fits, the EsCE and C1 components predict almost the same sequences, even though judging from the switching probabilities P_{12} and P_{21}, the block lengths are very different. The P_{12} and P_{21} values lie between 0.20 and 0.75, meaning that both states of the components are significant. Comparison of this with the simplest three-site model shows the weight fraction of the switching component in the low-melting fractions to be noticeably larger than the weight fraction of the Es_2 component.

In addition, constrained versions of the C1+Es+CE models were tested. The results of Busico et al.[42] suggest that the C1 component describes a site with one of the states equal to the Es component. In our case this results in a constraint $\sigma_{1,2} = \sigma_2$. Busico et al.[42] suggested that the similarity of the σ values, even without the constraint, means that the Es and C1 components describe the same site but in the C1 case the second state is accessible. The parameter values are likewise very similar in our case, and the constrained fit is almost as good as the unconstrained one ($\Delta\chi^2 \leq$ 3.0e-4). For both A and B, the constrained σ values (0.998 and 0.985, respectively) are close to the value

1.0 that was obtained by Busico et al. The other optimised model parameters have similar values as well, as shown in Table 5.

The similarity of the parameter values for the two samples increases the confidence of the C1+Es+CE result. This is not the case for model EsCE+Es+CE, however. Neither is there any clear indication that a similar constraint would work. Still, equally good fits are obtained if the P_r parameters in the CE and EsCE component are constrained ($P_{r,1} = P_{r,2}$). The CE component is, however, relatively unimportant in the model.

Table 5 *The optimised probabilities for model C1+Es+CE with constraint* $\sigma_{1,2} = \sigma_2$.

	A	B	Busico et al.[42]
$\sigma_{1,1}$	0.56	0.39	0.36
$\sigma_{1,2} = \sigma_2$	1.00	0.99	1.00
P_{12}	0.71	0.78	0.95
P_{21}	0.40	0.63	0.48
P_r	0.84	0.97	0.90

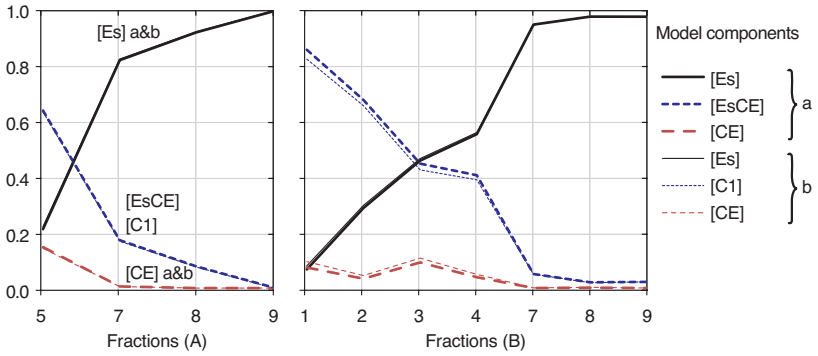

Figure 23 *EsCE+Es+CE (a) and C1+Es+CE (b) three-site model component weights for samples A and B.*

In the case of sample A, the best fit is obtained with the model proposed by Randall et al.[70] The differences between the three-site models are only marginal, however, and as shown in Figures 22 and 23, the changes in the component weights are small too. In addition, fewer sequences could be resolved for sample A because of its higher isotacticity. With sample A, therefore, it is not reasonable to try to fit more complex models. With sample B, also four-site models were evaluated. Because the CE1 component did not improve the three-site models with a switching component, the simpler CE component was used in the four-site models.

The addition of one CE1 component to the simplest three-site model results in the Es_1+Es_1+CE+CE1 model. Again the fit is slightly improved relative to the three-site models. Compared to the Es_1+Es_1+CE1 model in Figure 22 the additional syndiospecific CE component ($P_r = 1.00$) is mainly used to improve the fit in fraction 3.

To improve the current best-fit, an Es component was added to the EsCE(C1)+Es+CE models. The fits are slightly improved, but again the parameters of the first three components are not changed significantly. The fourth component (Es, $\sigma \sim 0.89$) mainly improves the fit in the fractions 2–4.

Figure 21 also shows the χ^2-fit obtained for the model C1+Es+CE1 with the sequence data calculated as a weighted sum of the data measured for the fractions. The number of parameters is reduced significantly in this fit, because the $n_{fr} \cdot n_c$ weights are not included (n_{fr} number of fractions, n_{c} number of components in the model). As shown in the figure, this fit gives the best χ^2 value. The parameter values do not, however, change significantly.

The small differences between the three- and four-site models, especially those with switching components, indicate that the available NMR data is not detailed enough to allow discrimination of these models. This is not surprising since ^{13}C NMR only provides information on relatively short sequences. Thus, from a stereoblock copolymer it is difficult, if not impossible, to obtain sufficiently detailed sequence data for reliable fits of the more complex three- and four-site models. This is the same conclusion that Randall et al.[70] were forced to draw. They subsequently tried to correlate the structure predicted by the different models with the results of crystallisation growth rate measurements.

A new approach is described in the following. Adopting an algorithm of Monte Carlo type, the fitted models are used to generate a set of chains, which are then compared with the results of the SSA measurements of the PP fractions.

Table 6 *Component weights for selected models from Table **4**.*

Model	*Sample*	*Fraction* / *Component*	**1**	**2**	***3***	**4**	**5**	**7**	**8**	**9**
Es+CE	A	[Es]					0.459	0.907	0.974	1.000
		[CE]					0.541	0.093	0.026	0.000
		$\chi^2 \cdot 10^2$					1.128	0.030	0.010	0.056
	B	[Es]	0.222	0.421	0.557	0.647		0.995	1.000	1.000
		[CE]	0.778	0.579	0.443	0.353		0.005	0.000	0.000
		$\chi^2 \cdot 10^2$	1.547	1.241	1.362	0.463		0.016	0.149	0.107
Es+CE1	A	[Es]					0.322	0.872	0.952	1.000
		[CE1]					0.678	0.128	0.048	0.000
		$\chi^2 \cdot 10^2$					0.270	0.040	0.015	0.010
	B	[Es]	0.105	0.326	0.476	0.583		0.969	0.995	0.995
		[CE1]	0.895	0.674	0.524	0.417		0.031	0.005	0.005
		$\chi^2 \cdot 10^2$	0.448	0.385	0.402	0.172		0.005	0.059	0.043
C1+CE	A	[C1]					0.628	0.126	0.051	0.000
		[CE]					0.372	0.874	0.949	1.000
		$\chi^2 \cdot 10^2$					0.287	0.028	0.017	0.004
	B	[C1]	0.887	0.682	0.544	0.445		0.088	0.061	0.060
		[CE]	0.113	0.318	0.456	0.555		0.912	0.939	0.940
		$\chi^2 \cdot 10^2$	0.499	0.304	0.466	0.206		0.108	0.031	0.088

Table 6 *Continued.*

Es_1+Es_2	A	$[Es_1]$					0.682	0.194	0.096	0.012
+CE		$[Es_2]$					0.152	0.796	0.904	0.988
		[CE]					0.167	0.009	0.000	0.000
			$\chi^2 \cdot 10^2$				0.092	0.009	0.010	0.001
	B	$[Es_1]$		0.763	0.672	0.402	0.385	0.053	0.012	0.029
		$[Es_2]$		0.000	0.209	0.415	0.510	0.941	0.977	0.971
		[CE]		0.237	0.120	0.182	0.106	0.006	0.012	0.000
			$\chi^2 \cdot 10^2$	0.348	0.265	0.217	0.105	0.005	0.032	0.035
Es_1+Es_2	A	$[Es_1]$					0.620	0.196	0.099	0.015
+CE1		$[Es_2]$					0.173	0.793	0.901	0.985
		[CE1]					0.207	0.011	0.000	0.000
			$\chi^2 \cdot 10^2$				0.083	0.010	0.010	0.001
	B	$[Es_1]$		0.614	0.589	0.308	0.335	0.065	0.017	0.042
		$[Es_2]$		0.000	0.201	0.420	0.503	0.927	0.967	0.958
		[CE1]		0.386	0.210	0.272	0.163	0.008	0.016	0.000
			$\chi^2 \cdot 10^2$	0.261	0.187	0.197	0.099	0.006	0.026	0.034
C1+Es	A	[C1]					0.635	0.169	0.076	0.000
+CE		[Es]					0.222	0.826	0.924	1.000
		[CE]					0.143	0.006	0.000	0.000
			$\chi^2 \cdot 10^2$				0.088	0.010	0.011	0.001
	B	[C1]		0.825	0.657	0.426	0.390	0.050	0.019	0.022
		[Es]		0.080	0.298	0.467	0.561	0.950	0.978	0.978
		[CE]		0.095	0.045	0.108	0.049	0.001	0.003	0.000
			$\chi^2 \cdot 10^2$	0.219	0.163	0.126	0.111	0.005	0.036	0.037
C1+Es	A	[C1]					0.144	0.795	0.910	1.000
+CE1		[Es]					0.633	0.192	0.090	0.000
		[CE1]					0.222	0.013	0.000	0.000
			$\chi^2 \cdot 10^2$				0.083	0.007	0.006	0.003
	B	[C1]		0.817	0.648	0.415	0.384	0.049	0.021	0.022
		[Es]		0.081	0.302	0.463	0.561	0.950	0.978	0.978
		[CE1]		0.102	0.051	0.122	0.055	0.000	0.001	0.000
			$\chi^2 \cdot 10^2$	0.222	0.170	0.119	0.111	0.005	0.036	0.037
EsCE+Es	A	[EsCE]					0.640	0.173	0.078	0.002
+CE		[Es]					0.212	0.821	0.922	0.998
		[CE]					0.148	0.006	0.000	0.000
			$\chi^2 \cdot 10^2$				0.088	0.010	0.011	0.001
	B	[EsCE]		0.859	0.678	0.448	0.406	0.051	0.021	0.022
		[Es]		0.067	0.289	0.459	0.555	0.949	0.978	0.978
		[CE]		0.074	0.034	0.092	0.039	0.000	0.001	0.000
			$\chi^2 \cdot 10^2$	0.223	0.166	0.117	0.105	0.005	0.037	0.037
EsCE+Es	A	[EsCE]					0.201	0.010	0.000	0.000
+CE1		[Es]					0.641	0.187	0.085	0.000
		[CE1]					0.158	0.803	0.915	1.000
			$\chi^2 \cdot 10^2$				0.085	0.007	0.006	0.002
	B	[EsCE]		0.862	0.679	0.451	0.408	0.050	0.021	0.022
		[Es]		0.067	0.289	0.459	0.555	0.950	0.978	0.978
		[CE1]		0.071	0.032	0.090	0.038	0.000	0.001	0.000
			$\chi^2 \cdot 10^2$	0.224	0.166	0.116	0.105	0.005	0.036	0.037

5.5 Monte Carlo Simulation of Crystallisable Sequence Lengths

The results of the best-fit calculations with the various two-, three- and four-site stochastic models lead more or less to the same conclusions as those of similar earlier studies. Even with the stereosequence data available for the fractions of the studied

samples, the three- and especially four-site models cannot be reliably distinguished. In introducing their model, Busico et al.[42] emphasized that the C1 component is in agreement with other independent experimental observations, like the increase in stereoregularity with decreasing monomer concentration, which can be explained with a mechanism analogous to that observed for the C_1-symmetric *ansa*-metallocenes. Even with the high-resolution ^{13}C NMR data they published, it is not possible to distinguish between the three-site models with a switching component (C1 or EsCE). Randall et al.,[70] on the other hand, emphasise that the model must agree with the crystallization growth rate data. They argue that the correct model must predict chains with long isotactic sequences between the defect-rich sequences. This kind of structure explains the similarity of the linear growth rates measured for PP fractions with different defect concentrations.[72] They conclude that the model C1+Es+CE1 is the only model to produce these kinds of sequences. Unfortunately, the data they present for this particular model is not completely reliable since the values presented in tables 1, 2 and 5 of their article do not agree. Their point is nevertheless valid; models *must* agree with the crystallisation data. The sequence structures predicted by the selected stochastic models from the previous section are compared in the following. A program based on the Monte Carlo algorithm was used for the purpose. From the probabilities of the models and the number average molar masses measured for the fractions, a set of chains was generated from which it is easy to calculate isotactic sequence lengths.

5.5.1 Comparison of Isotactic Sequence Lengths with SSA Melting Curves

In publication IV it was found that for the low-melting PP fractions (1-5) the SSA melting curve correlates with the longest isotactic sequences. This result allows us to compare the isotactic sequence lengths predicted by the stochastic models with the SSA melting curves of these fractions. A similar comparison is not possible for the high-melting fractions because the crystal structure depends, in addition to the chain structure, on the crystallisation conditions. Although it might be possible to calculate a melting curve on the basis of the crystallisable sequences and the crystallisation conditions, this is certainly not trivial for high-melting polypropylene samples with complex crystal morphology. Beigzadeh et al.[107] have demonstrated that a simple Monte Carlo algorithm can be used to generate a Crystaf curve in the case of ethylene-1-octene random copolymer samples. In these samples the crystallisable ethylene sequences are short, which ensures that chain-folding does not occur. The results of publication IV indicate that this is also the case with the low-melting PP fractions 1-5 (sample B). The crystal structure in these samples is most likely of the 'fringed micelle' type. These fractions, therefore, offer an excellent opportunity to test the models used in the previous section (5.4). Because the model probabilities were fitted to the data for the total samples (all fractions), the results obtained here should also be relevant for the high-melting fractions.

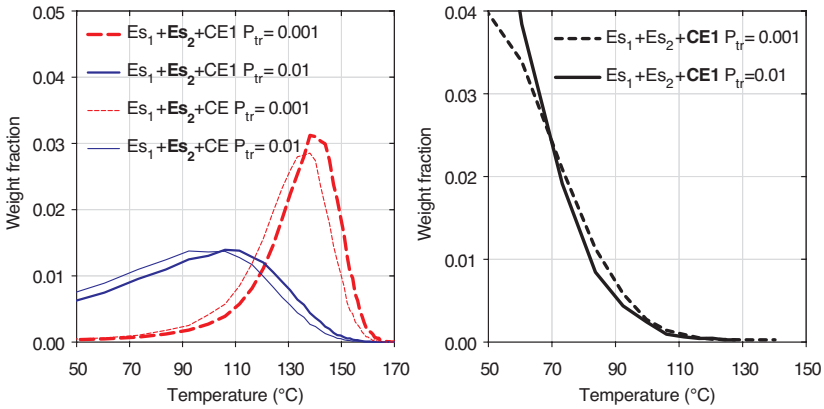

Figure 24 *Calculated weight fractions of chains with longest isotactic sequences long enough for the formation of crystallites that will melt at the specified temperature. Results shown for the model components CE1 and Es_2 in model Es_1+Es_2+CE1 and component Es_2 in model Es_1+Es_2+CE.*

The Es_1+Es_2+CE(1) model fits predict that the weight fraction of the highly isospecific Es_1 component is zero in the first fraction (Figure 22). This is in agreement with the DSC trace obtained for this fraction, which did not show a melting peak.[III] Indeed, it would be difficult to explain the presence of chains from this component in the amorphous fraction soluble in pentane at room temperature. Figure 24 shows the results of the Monte Carlo program for the other two components (Es_2 and CE1) of these models, two results for each component. These correspond to the simulations with chain termination probabilities (P_{tr}) equal to 0.01 and 0.001. For the low-melting fractions the termination probabilities were calculated from the number-average molar masses to lie between 0.005 and 0.008. Comparison of the CE and CE1 components in these models shows a clear difference. The CE component does not predict any chains with isotactic sequences longer than 14, which is the minimum length for crystallisable isotactic sequences.[126, 127] Thus, the CE component is not included in Figure 24. For the CE1 component the amount of these chains is 1.3%, but the longest sequences are still very short, only 25 monomers long (P_{tr} = 0.001). For the Es_2 component responsible for the isotactoid chains ($\sigma \approx 0.78$), the predicted longest sequences are significantly longer. With the termination probability 0.001, the longest sequences are 76 monomers, and 95% of the chains have isotactic sequences longer than 9.

Figure 25 shows the corresponding results for the three-site models with switching components. As discussed in the previous section, the weight fraction of the isotactoid component (switching component) is predicted to be much larger in three-site models with a switching component, than in the Es_1+Es_2+CE(1) models. The chain-end control component is predicted to account for less than 10% of the low-melting fractions. Comparison of Figures 24 and 25 reveals that the sequence distributions for the models

with a switching component differ significantly from what was predicted with the Es_1+Es_2+CE(1) models. The difference between the EsCE and C1 components is much smaller, within 5 °C. With P_{tr} value of 0.001, these values are about 30 °C lower than the prediction of the Es_2 component. The distributions are also clearly broader.

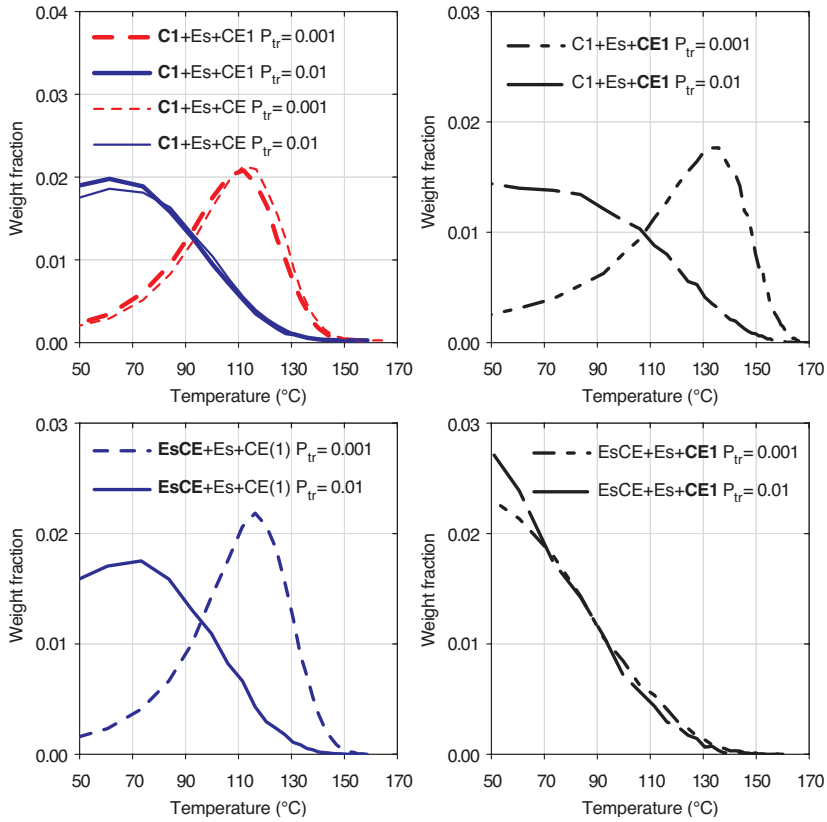

Figure 25 *Calculated weight fractions of chains with longest isotactic sequences long enough to form crystallites that will melt at the specified temperature. On the top, results for model C1+Es+CE1, and on the bottom, results for model EsCE+Es+CE1. The component shown in the graph is indicated in the model name with bold font*

.

The greatest difference in the "switching" models is in the chain-end control components, however. Again the CE component predicted only uncrystallisable chains and is therefore not shown in the figures. For both models, the CE1 components do predict chains with crystallisable sequences, but the distributions are very different in the two models. For the EsCE+Es+CE1 model, the longest sequences (P_{tr} = 0.001) are mainly of length that could produce crystallites with melting temperatures below 100 ºC. The lowest melting temperatures that were observed in the SSA thermograms were about 90 - 100 ºC.[IV] This means that the majority of these chains could not crystallise. For the C1-containing model, on the other hand, the CE1 component predicts sequences

with melting temperatures peaking at 135 ºC. A significant proportion of these chains are able to crystallise therefore.

From these results it is clear that the model C1+Es+CE1, proposed by Randall et al.,[70] predicts chain structures in best agreement with the experimental crystallisation data. The models with the CE component are clearly not in agreement with the crystallisation and fractionation results, as this component predicts only uncrystallisable chains. Of models with the CE1 component, the C1+Es+CE1 model predicts the largest fraction of crystallisable chains for the CE1 component and, in addition, the broad distribution predicted by the C1 component is in good agreement with the broad SSA melting curves.

A question still to be answered concerns the highly isospecific Es_1 component present in all the models. In all models the amount of this component in the low-melting fractions 2 to 5 is significant. It might be argued that these fractions contain the low molar mass fractions of this component. The more probable explanation, however, is that a $C1_1$+$C1_2$+CE1 model would be needed to predict the correct structure. As Busico et al.[42] have noted, the C1 and Es statistics tend to degenerate as the stereoregularity increases. Distinguishing these components is therefore beyond the limit of accuracy of the ^{13}C NMR experiments.

6 Conclusions

Propene polymerisation with a heterogeneous Ziegler-Natta catalyst system was studied with the aim of obtaining a better description of the active sites on the catalyst and in this way increasing understanding of the reactions important in polymer structure control. It was clear at the outset that a key area needing further study was the mechanisms of the electron donors, which are crucial in making supported catalyst systems highly stereospecific. The electron donors are known to influence the polymerisation in other ways as well. An active site that changes state upon coordination of an electron donor was found to explain the changes in the average activity, molar mass and isotacticity in a series of polymers prepared with different TEA/ED ratios.

Another topic of interest was the regioirregular insertion reaction, which had been proposed to influence both polymerisation activity and polymer structure. Molecular modelling methods were utilised because reactions on the catalyst surface and the catalyst system as such are difficult targets for study. DFT calculations showed that a strong agostic interaction between Ti of the active site and one of the hydrogens of the growing chain has a two-fold influence. An α-agostic interaction stabilises the transition structure and lowers the activation energy, while a β-agostic interaction effectively renders the site inactive for propene insertion. These results help in understanding the regiospecificity of the heterogeneous Z-N catalysts and the activating effect of hydrogen in propene polymerisation. As well, they explain the differences in ethene and propene polymerisations: in contrast to the result with propene, the β-agostic active site was found active for ethene insertion.

As another route for investigating the catalyst, a novel method of polymer structure analysis was developed. A recently introduced thermal calorimetric method, successive self-nucleation and annealing, was applied for the study of polypropylene. The results correlated well with TREF results, and the method offers a convenient way for qualitative estimation of the tacticity distribution.

Finally, ^{13}C NMR results were analysed using best-fit calculations of stochastic active-site models. To improve the confidence of the obtained fits, the results were checked by generating chains with a Monte Carlo algorithm. The C1+Es+CE1 model was found to give the best prediction of the ^{13}C NMR and SSA results.

7 References

1. Gobi International (www.gobi.co.uk), 20.5.2002
2. Natta G, Pino P, Corradini P, Danusso P, Mantica E, Mazzanti G, Moraglio G, *J. Am. Chem. Soc.* (1955), **77**, 1708
3. Giulio Natta, *From the Stereospecific Polymerization to the Asymmetric Autocatalytic Synthesis of Macromolecules*, Nobel Lecture 1963, http://nobelprize.org/
4. SRI Consulting (pep.sric.sri.com), Process Economics Program Report 128C, November 2002
5. Reichert KH, Meyer KR, *Macromol. Chem.* (1973), **169**, 163
6. Drent E, Budzelaar HM, *Chem. Rev.* (1996), **96**, 663
7. Younkin TR, Connor EF, Henderson JI, Friedrich SK, Grubbs RH, Bansleben DA, *Science* (2000), **287**, 460
8. *Isospecific Polymerization of Olefins with Heterogeneous Ziegler-Natta Catalysts*, Kissin YV, Springer-Verlag, New York, 1985
9. Dusseault JJA, Hsu CC, *J.M.S.-Rev. Macromol. Chem. Phys.* (1993), **C33**, 103
10. *Polypropylene Handbook*, Ed. by Moore EP, Jr. Hanser Publishers, München, 1996
11. Albizzati E, Giannini U, Collina G, Noristi L, Resconi L, in *Polypropylene Handbook*, Ed. by Moore EP, Jr. Hanser Publishers, München, 1996
12. Arzoumanidis GG. *Advances in Commercial Polypropylene Catalysts and Products*, SPO '91. Houston, Texas, September 24–26, 1991
13. Belgian Patents 785 332, 785 334 (1972) Montedison
14. European Patent 45 977 (1982) Montedison
15. U.S. Patent 4 971 937 (1990) HIMONT Incorporated
16. Cossee P, *J. Catal.* (1964), **3**, 80
17. Arlman EJ, *J. Catal.* (1964), **3**, 89
18. Arlman EJ, Cossee P, *J. Catal.* (1964), **3**, 99
19. Brookhart M, Green MLH, *J. Organomet. Chem.* (1983), **250**, 395
20. Boero M, Parrinello M, Terakura K, *Surf. Sci.* (1999), **438**, 1
21. Cavallo L, Guerra G, Corradini P, *J. Am. Chem. Soc.* (1998), **120**, 2428
22. Allegra G, *Makromol. Chem.* (1971), **145**, 235
23. Corradini P, Barone V, Fusco R, Guerra G, *Eur. Polym. J.* (1979), **15**, 1133

24. Venditto V, Guerra G, Corradini P, Fusco R, *Eur. Polym. J.* (1991), **27**, 45

25. Corradini P, Barone U, Fusco R, Guerra G, *Gazz. Chim. Ital.* (1983), **113**, 601

26. Boero M, Parrinello M, Weiss H, Hüffer S, *J. Phys. Chem. A* (2001), **105**, 5096

27. Chien JCW, Hu Y, *J. Polym. Sci., Part A: Polym. Chem.* (1989), **27**, 897

28. Chien JCW, Weber S, Hu Y, *J. Polym. Sci., part A: Polym. Chem.* (1989), **27**, 1499

29. Albizzati E, Giannini U, Balbontin G, Camurati I, Chadwick JC, Dall´occo T, Dubitsky Y, Galimberti M, Morini G, Maldotti A, *J. Polym. Sci., part A: Polym. Chem.* (1997), **35**, 2645

30. Chien JCW, Weber S, Hu Y, *J. Polym. Sci., part A: Polym. Chem.* (1989), **27**, 1499

31. Soga K, Ohnishi R, Sano T, *Polym. Bull.* (1982), **7**, 547

32. Giannini U, Giunchi G, Albizzati E, Barbè PC, *Recent Advances in Mechanistic and Synthetic Aspects of Polymerization*, NATO ASI Sect. 215, Ed. by Fontanille M, Guyot A, D. Reidel Publishing Co., 1987, p. 473

33. Härkönen M, Seppälä JV, Väänänen T, *Makromol. Chem.* (1991), **192**, 721

34. Yano T, Sakakibara Y, Sato H, Tamura M, Ikai S, Ikeuchi H, Yamashita J, Nakagava H, *Proceedings of the Eighth International Business Forum on Specialty Polyolefins*, Houston, 1998

35. Chadwick JC, Miedema A, Sudmeijer O, *Macromol. Chem. Phys.* (1994), **195**, 167

36. Barbe PC, Noristi L, Baruzzi G, *Makromol. Chem.* (1992), **193**, 229

37. Pino P, Rotzinger B, von Achenbach E, *Catalytic Polymerization of Olefins*, Ed. by Keii T, Soga K, Elsevier, Tokyo, 1986, p. 461

38. Soga K, Shiono T, Doi Y, *Makromol. Chem.* (1988), **189**, 1531

39. Barino L, Scordamaglia R, *Macromol. Theory Simul.* (1998), **7**, 407

40. Barino L, Scordamaglia R, *Macromol. Symp.* (1995), **89**, 101

41. Härkönen M, Seppälä JV, Salminen H, *Polym. J.* (1995), **27**, 256

42. Busico V, Cipullo R, Monaco G, Talarico G, Vacatello M, Chadwick JC, Segre AL, Sudmeijer O, *Macromolecules (*1999), **32**, 4173

43. Niu S, Hall MB, *Chem. Rev.* (2000), **100**, 353

44. Rappé AK, Skiff WM, Casewit CJ, *Chem. Rev.* (2000), **100**, 1435

45. Colbourn EA, Cox PA, Carruthers B, Jones PJV, *J. Mater. Chem.* (1994), **4**, 805

46. Puhakka E, Pakkanen TT, Pakkanen TA, *Surf. Sci.* (1995), **334**, 289

47. Boero M, Parrinello M, Terakura K, *J. Am. Chem. Soc.* (1998), **120**, 2746

48. Weiss H, Boero M, Parrinello M, *Macromol. Symp.* (2001), **173**, 137

49. Lin JS, Catlow CRA, *J. Mater. Chem.* (1993), **3**, 1217

50. Monaco G, Toto M, Guerra G, Corradini P, Cavallo L, *Macromolecules* (2000), **33**, 8953

51. Gale JD, Catlow CRA, Gillan MJ, *Topics in Catalysis* (1999), **9**, 235

52. Boero M, Parrinello M, Hüffer S, Weiss H, *J. Am. Chem. Soc.* (2000), **122**, 501

53. Puhakka E, Pakkanen TT, Pakkanen TA, Iiskola E, *J. Organomet. Chem.* (1996), **511**, 19

54. Puhakka E, Pakkanen TT, Pakkanen TA, *J. Mol. Catal. A: Chem.* (1997), **120**, 143

55. Puhakka E, Pakkanen TT, Pakkanen TA, *J. Phys. Chem. A* (1997), **101**, 6063

56. Puhakka E, Pakkanen TT, Pakkanen TA, *J. Mol. Catal. A: Chem.* (1997), **123**, 171

57. Härkönen M, Kuutti L, Seppälä JV, *Makromol. Chem.* (1992), **193**, 1413

58. Toto M, Morini G, Guerra G, Corradini P, Cavallo L, *Macromolecules* (2000), **33**, 1134

59. Scordamaglia R, Barino L, *Macromol. Theory Simul.* (1998), **7**, 399

60. Ritva Paukkeri, Licentiate thesis, University of Helsinki, 1992

61. Soares JBP, *Chem. Eng. Sci.* (2001), **56**, 4131

62. Paukkeri R, Lehtinen A, *Polymer* (1993), **34**, 4083

63. Coleman BD, Fox TG, *J. Chem. Phys.* (1963), **38**, 1065

64. Cheng HN, Babu GN, Newmark RA, Chien JCW, *Macromolecules* (1992), **25**, 6980

65. Busico V, Cipullo R, *Prog. Polym. Sci.* (2001), **26**, 443

66. Busico v, Cipullo R, Corradini P, Landriani L, Vacatello M, Segre AL, *Macromolecules* (1995), **28**, 1887

67. Inoue Y, Itabashi Y, Chûjô R, Doi Y, *Polymer* (1984), **25**, 1640

68. Doi Y, *Makromol. Chem., Rapid Commun*. (1982), **3**, 635

69. Chûjô R, Kogure Y, Väänänen T, *Polymer* (1994), **35**, 339

70. Randall JC, Alamo RG, Agarwal PK, Ruff CJ, *Macromolecules* (2003), **36**, 1572

71. Cheng HN, *Makromol. Chem., Theory Simul.* (1992), **1**, 415

72. Alamo RG, Blanco JA, Agarwal PK, Randall JC, *Macromolecules* (2003), **36**, 1559

73. Marigo A, Marega C, Saini R, Camurati I, *J. Appl. Polym. Sci. (*2000), **79**, 375

74. Alamo RG, Lucas JC, Mandelkern L, *Polym. Preprints* (1994), **35**, 406

75. Hamley IW, *Introduction to Soft Matter: Polymers, Colloids, Amphiphiles and Liquid Crystals*, John Wiley & Sons, Ltd, Chichester, 2002, p. 104

76. Yamada K, Matsumoto S, Tagashira K, Hikosaka M, *Polymer* (1998), **39**, 5327

77. Lauritzen Jr J. I., Hoffman J. D., *J. Res. Natl. Bur. Stand. A* (1961), **64**, 73

78. Hoffman J. D., Lauritzen Jr J. I., *J. Res. Natl. Bur. Stand. A* (1961), **65**, 297

79. Sadler D, *Polymer* (1983), **24**, 1401

80. Keller A., Cheng S. D. Z., *Polymer* (1998), **39**, 4461

81. Strobl G, *Eur. Phys. J. E* (2000), **3**, 165–183

82. Lotz B, *Eur. Phys. J. E* (2000), **3**, 185

83. Flory PJ, *Trans. Faraday Soc.* (1955), **51**, 848

84. Soares JBP, Hamielec AE, *Macromol. Theory Simul.* (1995), **4**, 305

85. Bicerano J, *J.M.S. – Rev. Macromol. Chem. Phys.* (1998), **3**, 391

86. Cheng SZD, Janimak JJ, Zhang A, Hsieh ET, *Polymer* (1991), **32**, 648

87. Viville P, Daoust D, Jonas AM, Nysten B, Legras R, Dupire M, Michel J, Debras G. *Polymer* (2001), **42**, 1953

88. Hauser G, Schmidtke J, Strobl G, *Macromolecules* (1998), **31**, 6250

89. Sanchez IC, Eby RK, *J. Res. Nat. Bur. Stand. A, Phys. Chem.* (1973), **77**, 353

90. Yamada K, Matsumoto S, Tagashira K, Hikosaka M, *Polymer* (1998), **39**, 5327

91. Iijima M, Strobl G, *Macromolecules* (2000), **33**, 5204

92. Yamada K, Matsumoto S, Tagashira K, Hikosaka M, *Macromolecules* (2003), **36**, 4790

93. Ogawa T, Hoshino S, *J. Appl. Polym. Sci.* (1973), **17**, 2235

94. Kawamura H, Hayashi T, Inoue Y, Chûjô R, *Macromolecules* (1989), **22**, 2181

95. Paukkeri R, Iiskola E, Lehtinen A, Salminen H, *Polymer* (1994), **35**, 2636

96. Paukkeri R, Väänänen T, Lehtinen A, *Polymer* (1993), **34**, 2488

97. Lehtinen A, Paukkeri R, *Macromol. Chem. Phys.* (1994), **195**, 1539

98. Wild L, Ryle T, Knobeloch D, Peat I, *J. Polym. Sci., Polym. Phys. Ed*. (1982), **20**, 441

99. Wild L, *Trends Polym. Sci.* (1993), **1**, 50.

100. Monrabal B, *Macromol. Symp.* (1996), **110**, 81

101. Chen F, Shanks RA, Amarasinghe G, *Polymer* (2001), **42**, 4579

102. Adisson E, Ribeiro M, Deffieux A, Fontanille M, *Polymer* (1992), **33**, 4337

103. Müller AJ, Hernández ZH, Arnal ML, Sánchez JJ, *Polym. Bull. (*1997), **39**, 465

104. Xu J, Feng L, Yang S, Yang Y, Kong X, *Eur. Polym. J.* (1998), **34**, 431

105. Lodefier P, Daoust D, Jonas AM, Legras R, *Macromol. Symp.* (1999), **148**, 59

106. Lodefier P, Jonas AM, Legras R, *Macromolecules* (1999), **32**, 7135

107. Beigzadeh D, Soares JBP, Duever TA, *J. Appl. Polym. Sci. (*1999), **80**, 2200

108. Wild L, Chang S, Shankernarayanan MJ, *Polym. Prepr.* (1990), **31**, 270

109. Gabriel C, Lilge D, *Polymer* (2001), **42**, 297

110. Delley B, *J. Chem. Phys.* (1990), **92**, 508

111. Becke D, *Phys. Rev. A* (1988), **38**, 3098

112. Lee C, Yang W, Parr RG, *Phys. Rev. B* (1988), **37**, 785

113. Price FP in *Markov Chains and Monte Carlo Calculations in Polymer Science*, Ed. by Lowry GG, Marcel Dekker Inc., New York 1970, p. 187-257

114. Press WH, Teukolsky SA, Vetterling WT, Flannery BP, *Numerical Recipes in C*, 2nd Edition, Cambridge University Press 1999, p. 408

115. ANSI C version of DONLP2 (14.5.2003), P. Spellucci, http://www.netlib.org/

116. Keii T, Suzuki E, Tamura M, Murata M, Doi Y, *Makromol. Chem.* (1982), **183**, 2285

117. Keii T, Terano M, Kimura K, Ishii K, in *Transition Metals And Organometallics as Catalysts for Olefin Polymerization,* Ed. by Kaminsky W, Sinn H, Springer-Verlag, Berlin, 1988, p. 3

118. Moscardi G, Piemontesi F, Resconi L, *Organometallics* (1999), **18**, 5264

119. Spitz R, Masson P, Bobichon C, Guyot A, *Makromol. Chem.* (1988), **189**, 1043

120. Chadwick JC, van Kessel GMM, Sudmeijer O, *Macromol. Chem. Phys.* (1995), **196**, 143

121. de Carvalho ABM, Gloor PE, Hamielec AE, *Polymer* (1990), **31**, 1294

122. Gabriel C, Lilge D, *Polymer* (2001), **42**, 297

123. Randall JC, *Macromolecules* (1997), **30**, 803

124. Cheng HN, *Makromol. Chem., Theory Simul.* (1992), **1**, 415

125. Busico V, Cipullo R, Corradini P, De Biasio R, *Macromol. Chem. Phys.* (1995), **196**, 491

126. Collette JW, Ovenall DW, Buck WH, Ferguson RC, *Macromolecules* (1989), **22**, 3858

127. Madkour TM, Mark JE, *Macromol. Theory Simul.* (1998), **7**, 6